



Biological production in the Bellingshausen Sea from oxygen-to-argon ratios and oxygen triple isotopes

K. Castro-Morales^{1,*}, N. Cassar^{2,**}, D. R. Shoosmith³, and J. Kaiser¹

¹School of Environmental Sciences, University of East Anglia, Norwich, UK

²Geosciences Department, Princeton University, Princeton, USA

³British Antarctic Survey, Cambridge, UK

* now at: Alfred Wegener Institute Helmholtz Centre for Polar and Marine Research, Bremerhaven, Germany

** now at: Division of Earth and Ocean Sciences, Nicholas School of the Environment, Duke University, Durham, NC, USA

Correspondence to: K. Castro-Morales (karel.castro-morales@awi.de)

Received: 15 October 2012 – Published in Biogeosciences Discuss.: 15 November 2012

Revised: 27 February 2013 – Accepted: 14 March 2013 – Published: 5 April 2013

Abstract. We present estimates of mixed-layer net community oxygen production (N) and gross oxygen production (G) of the Bellingshausen Sea in March and April 2007. N was derived from oxygen-to-argon (O_2/Ar) ratios; G was derived using the dual-delta method from triple oxygen isotope measurements. In addition, O_2 profiles were collected at 253 CTD stations. N is often approximated by the biological oxygen air–sea exchange flux (F_{bio}) based on the O_2/Ar supersaturation, assuming that significant horizontal or vertical fluxes are absent. Here we show that the effect of vertical fluxes alone can account for F_{bio} values < 0 in large parts of the Bellingshausen Sea towards the end of the productive season, which could otherwise be mistaken to represent net heterotrophy. Thus, improved estimates of mixed-layer N can be derived from the sum of F_{bio} , F_e (entrainment from the upper thermocline during mixed-layer deepening) and F_v (diapycnal eddy diffusion across the base of the mixed layer). In the winter sea ice zone (WSIZ), the corresponding correction results in a small change of $F_{bio} = (30 \pm 17) \text{ mmol m}^{-2} \text{ d}^{-1}$ to $N = (34 \pm 17) \text{ mmol m}^{-2} \text{ d}^{-1}$. However, in the permanent open ocean zone (POOZ), the original F_{bio} value of $(-17 \pm 10) \text{ mmol m}^{-2} \text{ d}^{-1}$ gives a corrected value for N of $(-2 \pm 18) \text{ mmol m}^{-2} \text{ d}^{-1}$. We hypothesize that in the WSIZ, enhanced water column stability due to the release of freshwater and nutrients from sea ice melt may account for the higher N value. These results stress the importance of accounting for physical biases when estimating mixed-layer marine productivity from in situ O_2/Ar ratios.

1 Introduction

The Bellingshausen Sea is one of the less explored regions in Antarctica. It is located in the West Antarctic Peninsula (WAP) region and includes one of the major shelf areas in the Southern Ocean (SO), characterized by high phytoplankton biomass and high concentrations of chlorophyll a and iron in surface waters (Holm-Hansen et al., 2005). Factors such as water column stability, irradiance and nutrient input are responsible for the high biomass and complex phytoplankton community in the region (Boyd et al., 1995; Garibotti et al., 2003; Smith and Comiso, 2008; Vernet et al., 2008).

During the last decade, the waters of the WAP have experienced a mean increase of 0.5°C in the top 100 m of the water column with the largest changes in winter (Holland et al., 2010; Meredith and King, 2005; Meredith et al., 2010; Montes-Hugo et al., 2010). Particularly, the Bellingshausen Sea has been affected by this rapid oceanic and atmospheric warming; both of which have had consequences on its ice shelves, such as Wilkins Ice Shelf (Graham et al., 2011). The invasion of relatively warm circumpolar deep water (CDW) onto the continental shelf is likely to be the main driver for ice shelf thinning and sea ice melting in the region (Jacobs et al., 1996; Jenkins and Jacobs, 2008). Furthermore, climate change in the SO may have led to increased wind speeds (Le Quéré et al., 2007) with implications for sea ice formation and persistence (Cook et al., 2005). A stronger mixing regime can affect the structure of the water column, nutrient supply by upwelling, as well as phytoplankton abundance

and community composition (Arrigo et al., 2008). Warming can also drive deoxygenation, to which the Southern Ocean is particularly susceptible (Keeling and Garcia, 2002; Matear et al., 2000).

Because of the fast changes occurring in waters of the WAP, it is important to evaluate the current state of the marine communities in the region, particularly changes in marine productivity. Previous estimates of marine biological production in the Bellingshausen Sea were based on discrete measurements of ^{14}C assimilation, chlorophyll *a* concentrations, seasonal inorganic nutrient deficits and phytoplankton abundance (i.e., Boyd et al., 1995; Garibotti et al., 2003; Serebrennikova and Fanning, 2004; Turner and Owens, 1995; Vernet et al., 2008). Marine production from remotely sensed ocean color in the Southern Ocean has been also performed (Arrigo et al., 2008).

Here we present estimates of mixed-layer average net community oxygen production (N) and gross oxygen production (G) in the Bellingshausen Sea during the period of February to April 2007, based on continuous ship measurements of O_2/Ar ratios and discrete samples for oxygen triple isotopes.

The O_2/Ar and oxygen triple isotope techniques have been applied before in the SO (Cassar et al., 2007, 2011; Guéguen and Tortell, 2008; Reuer et al., 2007; Tortell and Long, 2009), including the Bellingshausen Sea (Hendricks et al., 2004; Huang et al., 2012). O_2/Ar only has been used in the Ross Sea (Tortell et al., 2011) and Amundsen Sea (Tortell et al., 2012). Hendricks' productivity estimates were based on discrete sampling away from the continental shelf, but did not resolve the direct influence of sea ice along the shelf. The study area of Huang et al. (2012) was located in the Palmer Long-Term Ecological Research (LTER) region, north of our area of study, and comprised a coarser grid of hydrographic stations than the present study, mainly outside the sea ice zone.

The O_2/Ar approach is used to measure the biological oxygen air–sea exchange flux, F_{bio} . Neglecting the influence of vertical and horizontal transport on the mixed-layer O_2 mass balance, N is approximated by F_{bio} (Kaiser et al., 2005). Previous studies in the Southern Ocean did not try to establish whether the observed negative F_{bio} values were due to mixing with undersaturated waters or whether they reflected actual heterotrophy (Hendricks et al., 2005; Reuer et al., 2007).

Recent observations in other world's oceans have concluded that the consideration of physical effects, such as entrainment of subsurface waters into the mixed layer, in the productivity estimates using the O_2 budget approach must be taken into account (i.e., Hamme and Emerson, 2006; Luz and Barkan, 2009; Nicholson et al., 2012). Mixing and entrainment processes at the base of the mixed layer can lead to underestimation of N by the O_2 budget by as much as 80 % in the subtropical gyres (Nicholson et al., 2012). In the present study we explore the influence of entrainment of water from the upper thermocline during mixed-layer deepening and di-

apycnal eddy diffusion across the base of the mixed layer on the mixed-layer O_2 mass balance. The influence of horizontal transport is neglected because strong currents and fronts and associated gradients are absent in the interior of the Bellingshausen Sea, with the only prominent front centered at 67°S and 85°W off our study area (Pollard et al., 1995). Although the derivation of G using the oxygen triple isotope technique may be affected by the same physical processes (Hendricks et al., 2005), here we only investigate their influence on N . We also investigate variations in F_{bio} in relation to the marginal ice zone (MIZ) and the stability of the water column. Finally, we compare our results to previous productivity estimates in the region.

2 Area of study

The present study was carried out during 38 days (3 March to 9 April 2007) onboard RRS *James Clark Ross* within the framework of the British Antarctic Survey's ACES-FOCAS project (Antarctic Climate and the Earth System-Forcing from the Oceans, Clouds, Atmosphere and Sea-ice). The surveyed section in the Bellingshausen Sea lies between 66° and 73°S and between 66° and 93°W . It is the southernmost limit of the WAP, with the latter extending to the northern tip of the peninsula and to the shelf break in the west (Ducklow et al., 2007). The sampling period coincided with the transition from summer to autumn, late melting winter ice and the formation of new ice.

The Bellingshausen Sea is located in the Antarctic Zone (AZ), in a transition region between the Antarctic continental shelf, the shelf break and the open ocean, often delimited by the 3000 m isobath (Fig. 1). Two zones can be distinguished within the AZ: the sea ice zone, which is predominantly seasonal with about 80 % of the first-year ice that melts back each summer (Sturm and Masson, 2010); and the permanent open ocean zone (POOZ), where sea ice is absent year-round. In this work we will refer to the sea ice zone as the winter sea ice zone (WSIZ) hereinafter in order to refer specifically to a region that is ice covered in winter only and mostly free of ice during summer.

The MIZ separates the WSIZ and POOZ (Hiraike and Ikeda, 2009; Vernet et al., 2008). In the Bellingshausen Sea, the MIZ can normally be found between 65°S and 70°S and between 80°W and 87°W (Turner and Owens, 1995), about 100 km offshore during summer and 200 km offshore during winter.

The hydrography of the Bellingshausen Sea is influenced by bottom topography, coastlines and sea ice seasonality. The Antarctic Circumpolar Current (ACC), flowing around the Antarctic continent, supplies CDW to the shelf in this region. The formation and transport of surface water masses varies seasonally, and is dependent mainly on the freshwater input from melting ice and vertical mixing.

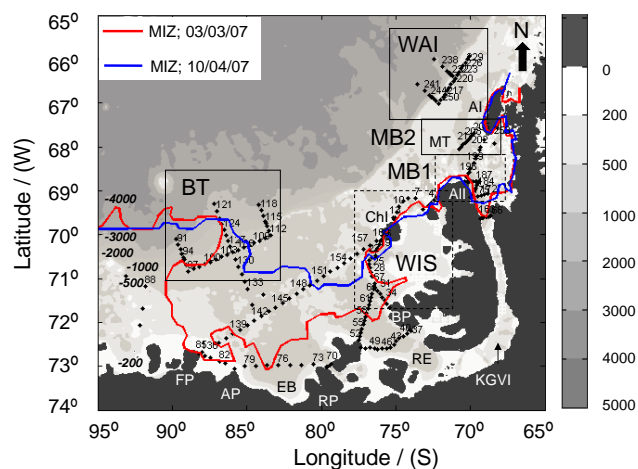


Fig. 1. Area of study for cruise JR165 in the Bellingshausen Sea during summer 2007. Black dots indicate the location of the CTD stations occupied during the cruise. The location of the marginal ice zone (MIZ) from AMSR-E satellite images is also shown at the beginning and end of the cruise. Main coastal features (from west to east): FP, Fletcher Peninsula; AP, Allison Peninsula; EB, Eltanin Bay; RP, Rydberg Peninsula; RE, Ronne Entrance; BP, Beethoven Peninsula; KGVI, King George VI Sound; ChI, Charcot Island; All, Alexander Island; MT, Marguerite Trough; AI, Adelaide Island. Stations in the WSIZ are outlined by dashed-line rectangles: WIS, Wilkins Ice Shelf and MB1, Marguerite Bay 1; stations in the permanent open ocean zone (POOZ) by solid line rectangles: BT, Belgica Trough; MB2, Marguerite Bay 2 and WAI, west of Adelaide Island.

The interaction between glacial water, sea ice melt water (MW) and oceanic waters in the Bellingshausen Sea affects the biological productivity distribution. In the Bellingshausen Sea, the main water masses are the following: CDW, entering the shelf as an extension of the ACC; AASW (Antarctic surface water), filling the upper 200 m during summer and autumn and extending from the Antarctic continent to the Antarctic Polar Front (APF); WW (winter water), formed during winter below the packed ice and dominating the deep mixed layer (i.e., > 100 m) until early spring, when it is replaced by AASW; and MW released during summer from the coast and shelf areas covered with ice. Its release stabilizes the water column during the peak of the growing season (Serebrennikova and Fanning, 2004; Smith et al., 1999).

Through light availability and nutrient release, sea ice affects biological community composition and abundance (Garibotti et al., 2005a; Serebrennikova and Fanning, 2004; Vernet et al., 2008). During early spring, iron and algae are released from the melting sea ice (Hopkinson et al., 2007). This process, and the presence at the surface of nutrient-rich WW in a stratifying water column, is believed to lead to the spring phytoplankton blooms (Boyd et al., 2000; Martin et al., 1991) especially near the MIZ.

During the peak growing season in summer (January), chlorophyll *a*, carbon biomass and phytoplankton abundance are highly variable (Garibotti et al., 2005a; Smith et al., 2008; Vernet et al., 2008). At this stage, blooms persist for several weeks and diatom communities dominate the shelf waters of the Bellingshausen Sea (Garibotti et al., 2005a, 2003; Mura et al., 1995; Smith et al., 2008).

As the growing season evolves, silicate and nitrate become depleted. Iron concentration also decreases (< 0.1 nM), further limiting phytoplankton growth (Smith et al., 2000). By March, seasonal heating and mixing due to wind stress further erode the WW replaced by the AASW. This is especially the case in the POOZ.

From November to March (late spring to summer) MW dominates close to the coast. During these months, weaker winds and the stratified water column result in shallow summer mixed layers (< 50 m) (Holm-Hansen et al., 2005). In the WSIZ, MW replaces WW in the mixed layer, but leaves a remnant of WW underneath (Garibotti et al., 2003; Vernet et al., 2008), storing the properties of the upper water column of the preceding winter. This has been observed previously in the WAP (Serebrennikova and Fanning, 2004) and in the MIZ of the Australian sector of the SO, where elevated nutrient content reflects remnant winter mixed layer (Ishii et al., 2002).

3 Methods

3.1 Hydrographic stations and underway measurements

Vertical profiles of temperature (θ), salinity (S) and dissolved oxygen concentration ($c(\text{O}_2)$) were obtained at 253 CTD stations (Fig. 1). S was measured with two conductivity sensors calibrated against discrete samples analyzed onboard with a Guildline Autosal 8400B. θ and $c(\text{O}_2)$ were measured with high-precision digital reversing thermometers (Sea-Bird SBE35) and two O_2 sensors (CTD- O_2 ; Sea-Bird SBE43), respectively, mounted on the rosette. The O_2 sensors responded less rapidly than the temperature and conductivity CTD sensors. Sensor lags for the two O_2 sensors were 8 s and 9 s, respectively, and were established by finding the lag time that minimized the root-mean-squared differences between downcast and upcast. One of the O_2 sensors proved to be more stable and was selected for calibration. O_2 profiles in deep casts (> 1000 m) have been reported to be affected by pressure hysteresis (Sea-Bird Electronics, 2010). However, we observed little hysteresis on 38 of our CTD profiles which reached depths greater than 1000 m. A correction had to be applied to the pressure sensor, which amounted to the following values: stations 0–21: –1.21 dbar; 22–85: –0.71 dbar; 86–164: –1.05 dbar; 165–253: –0.80 dbar. All measurements were vertically averaged in steps of 2 dbar.

A total of 276 discrete seawater samples from the CTD profiles (and 186 from the continuous underway supply, see below) were collected for O₂ sensor calibration and analyzed onboard using whole-bottle Winkler titration (Dickson, 1996) with photometric end-point detection. The calibration was made using the upcast CTD values at the density levels where the bottles were closed. We obtained a repeatability of 0.29 μmol kg⁻¹ for 76 duplicate samples. The average difference between non-calibrated CTD-O₂ and Winkler data was (+3.9 ± 3.2) μmol kg⁻¹, and after calibration was (+1.1 ± 3.9) μmol kg⁻¹.

Supporting physical variables were also measured using the underway seawater sampling system, which has an intake at a nominal depth of 6 m near the bow of the ship. Sea surface temperature (θ_0) was measured directly at the intake; sea surface salinity (S_0) and O₂ concentrations were recorded further downstream, using a Sea-Bird Electronics (SBE) thermosalinograph and an O₂ optode (Model 3835, Aanderaa Instruments AS, Bergen, Norway), respectively. The delay from the sample intake to the measurement point for salinity and oxygen was 2 min. This was corroborated by the change in temperature recorded in the optode from warm (above 10 °C) to close to seawater freezing point (-1.8 °C) in regions with ice surrounding. These events were clear during a transition of no underway water flow to flow restoration at a time recorded by the flowmeter located at the underway intake. The delay caused a warming of (0.65 ± 0.1) °C. S_0 was calibrated using discrete samples analyzed onboard in the same way as for the CTD sensor. A constant offset of 0.0337 was added in order to correct the underway salinity record. The underway O₂ measurements were calibrated against discrete samples collected from the underway system. The latter were analyzed onboard by Winkler titration, in the same way as for the CTD-O₂ calibration. The oxygen concentration from the optode was calibrated following Kaiser et al. (2005). The average difference between Winkler data and noncalibrated underway O₂ was (-0.1 ± 2.8) μmol kg⁻¹, and after optode calibration the difference was reduced to (0.0 ± 0.6) μmol kg⁻¹. From the meteorological station onboard, we obtained barometric pressure (P) and wind speed. The latter was corrected to 10 m above sea level (u_{10}) (Johnson, 1999).

To calculate the biological oxygen air-sea exchange flux and to estimate net community production, we continuously measured O₂/Ar ratios in the underway sampling system by membrane inlet mass spectrometry (MIMS) (Kaiser et al., 2005; Kana et al., 1994; Tortell, 2005). Seawater from the ship's underway system was pumped through a chamber with a Teflon AF membrane (Random Technologies). The membrane was connected to the vacuum of a quadrupole mass spectrometer (Pfeiffer Vacuum Prisma). Temperature effects and water vapor pressure variations in the measurements were reduced by keeping the membrane in a water bath at a constant temperature of 0 °C. O₂ (m/z 32) to Ar (m/z 40) ion current ratio measurements were made every 6 s with a

short-term (2 min) repeatability of 0.05 %. Our continuous high-frequency O₂/Ar measurements allow us to identify marine productivity gradients and large variability at high spatial (1 km) and temporal (3 min) resolution.

For calibration of the O₂/Ar measurements, discrete samples were drawn into evacuated bottles. After the cruise, liquid and gas phase had equilibrated. Most of the water was drained and water vapor, N₂ and CO₂ were removed using an extraction line comprising cryogenic and gas-chromatographic purification steps. The remaining O₂ and Ar mixture was analyzed by isotope ratio mass spectrometry (IRMS) (Thermo Finnigan MAT 252) for ion beam intensities at m/z 32 and 40 using peak jumping (Luz and Barkan, 2000). To derive gross photosynthetic O₂ production from oxygen triple isotopes, the same samples were used to measure the relative ¹⁷O/¹⁶O and ¹⁸O/¹⁶O isotope ratio differences between dissolved O₂ and air O₂ (¹⁷ δ and ¹⁸ δ).

3.2 Sea-to-air O₂ flux (F_g) calculation

The supersaturation of O₂, $\Delta(O_2)$ is given by

$$\Delta(O_2) = \frac{c(O_2)}{c_{eq}(O_2)} - 1, \quad (1)$$

where $c(O_2)$ is the measured O₂ concentration and $c_{eq}(O_2)$ is the O₂ concentration at equilibrium with the atmosphere, calculated at in situ temperature, salinity and pressure (Garcia and Gordon, 1992, 1993). $\Delta(O_2)$ can be negative, in which case it represents an oxygen undersaturation.

The flux of oxygen through the air-sea interface (F_g) is calculated from

$$F_g = k_w c_{eq}(O_2) \Delta(O_2), \quad (2)$$

where k_w is the O₂ gas exchange coefficient. Positive F_g values represent a net flux from the ocean to the atmosphere. k_w was parameterized in terms of wind speed following Sweeney et al. (2007), averaged for 60 days prior to sampling using the method suggested by Reuer et al. (2007), and the mixed-layer depth defined by the vertical distribution of O₂ following Castro-Morales and Kaiser (2012). Wind speeds were obtained from the European Centre for Medium-Range Weather Forecasts (ECMWF, 6 h resolution, operational analysis, 1° × 1°) and varied during the cruise from 1 to 27 m s⁻¹, with a mean of 8 m s⁻¹. The root-mean-squared difference between ship winds (u_{10}) and ECMWF winds was 2.5 m s⁻¹. The absolute difference between the ECMWF wind product and u_{10} was (0.8 ± 2.4) m s⁻¹. Considering the mixed-layer depths and gas exchange coefficients, the residence time of O₂ in the upper mixed layer was on average 25 days.

3.3 Biological O₂ flux (F_{bio}) determination from O₂/Ar ratios

The O₂/Ar method to estimate net community production exploits the similar solubility characteristics of these two gases.

Basically, it “corrects” the O_2 supersaturation for physical effects due to temperature, salinity or pressure changes and bubble effects. The biological oxygen supersaturation, $\Delta(O_2/Ar)$, is defined as the relative deviation of the O_2/Ar ratio in the sample to the O_2/Ar ratio at equilibrium with the atmosphere (Craig and Hayward, 1987; Emerson et al., 1995; Kaiser et al., 2005; Spitzer and Jenkins, 1989),

$$\Delta(O_2/Ar) = \frac{c(O_2)/c(Ar)}{c_{eq}(O_2)/c_{eq}(Ar)} - 1, \quad (3)$$

where $c_{eq}(O_2)$ and $c_{eq}(Ar)$ are calculated as a function of temperature and salinity (Garcia and Gordon, 1992, 1993; Hamme and Emerson, 2004).

The biological oxygen air–sea exchange flux is defined as

$$F_{bio} = k_w c_{eq}(O_2) \Delta(O_2/Ar). \quad (4)$$

A positive F_{bio} value corresponds to outgassing of biologically produced O_2 from the mixed layer.

To estimate the standard error in our measurements, we measured aliquots of air-saturated water prepared and analyzed in the laboratory in the same way as the seawater samples. A total of 11 air-saturated water measurements gave a standard error in $\Delta(O_2/Ar)$ of 0.05 %, which does not contribute significantly to the overall uncertainty in F_{bio} . The uncertainty in F_{bio} is mainly due to the wind-speed-dependent parameterization of the gas transfer coefficient (k_w), which according to Sweeney et al. (2007) solely accounts for 15 %.

At steady state and in the absence of mixing, F_{bio} is interpreted as biological net community production N averaged over the residence time of water in the mixed layer, but this does not account for physical mixing process interpretation. We here quantify at least part of these processes by estimating the influence of entrainment of thermocline waters when the mixed layer deepens (Sect. 3.4) and vertical eddy diffusion as a result of the oxygen concentration gradient of oxygen across the base of the mixed layer (Sect. 3.5).

To calculate net community production in terms of carbon ($N(C)$), N was divided by the photosynthetic quotient of 1.4 for nitrate-based production (i.e., $N = 1.4 \times N(C)$) (Laws, 1991). ^{14}C net primary production, $G(^{14}C)$ (or $N(^{14}C)$), was derived assuming $G = 2.7 N(^{14}C)$ (Bender et al., 1999; Marra, 2002).

3.4 Entrainment of $O_2(F_e)$ due to changes in the depth of the mixed layer

Previous approaches to estimate F_e (Emerson, 1987; Emerson et al., 2008) have used the concentration difference between thermocline and mixed layer. However, it is unclear how this concentration difference should be computed. Therefore, we derive the corresponding entrainment flux (F_e) in Appendix A, based on the O_2 concentration gradient below the mixed layer:

$$F_e = -\frac{1}{2} \frac{(\Delta z_{mix})^2}{\Delta t} \frac{\partial c(O_2)}{\partial z} \Big|_{oxy}, \quad (5)$$

where the partial derivative is the gradient of oxygen in the oxycline, and $\Delta z_{mix} = z_{mix, 1} - z_{mix, 0}$ is the thickness of the entrained water column. For practical reasons we chose $z_{mix, 0}$ to correspond to 30 days before the cruise; $z_{mix, 1}$ corresponds to the mixed layer at the sampling time (i.e., z_{mix}). Positive Δz_{mix} values represent deeper mixed layers than 30 days before our sampling time. Negative Δz_{mix} values (mixed-layer shoaling) are ignored because they do not change the O_2 concentration. Positive F_e values represent a decrease of mixed-layer O_2 concentration due to entrainment of low-oxygenated waters.

The depth of the mixed layer 30 days before sampling was estimated from the monthly climatology of de Boyer Montégut et al. (2004). To correct for the difference between climatological and observed mixed-layer depths, 8 m were subtracted from the climatological values (Castro-Morales and Kaiser, 2012).

3.5 Diapycnal eddy diffusion (F_v) across the base of the mixed layer

F_v is calculated from Fick’s first law of diffusion following:

$$F_v = -K_z \frac{\partial c(O_2)}{\partial z} \Big|_{oxy}. \quad (6)$$

For K_z (eddy diffusivity coefficient) we used a mean value of $\leq 1.0 \times 10^{-5} \text{ m}^2 \text{ s}^{-1}$ based on the study of Howard et al. (2004) in Marguerite Bay during the Southern Ocean Global Ecosystem Dynamics program (GLOBEC) in autumn and winter 2001. The selected K_z value is in close agreement to mean effective value of $1.1 \times 10^{-5} \text{ m}^2 \text{ s}^{-1}$ derived by Law et al. (2003) during the SF₆ tracer release Southern Ocean Iron Enrichment Experiment (SOIREE) in summer 1999 in the Australian sector of the SO (Law et al., 2003). The minimum and maximum wind speed values recorded during SOIREE (from 5 to 12 m s^{-1}) were similar to the values recorded during our cruise (from 4.6 to 8 m s^{-1}). The square of the buoyancy frequency (ν^2) during SOIREE was 10^{-3} s^{-2} for the seasonal pycnocline and up to 10^{-5} s^{-2} in the mixed layer towards the end of the experiment. During GLOBEC, the buoyancy frequency (ν^2) was $< 10^{-4} \text{ s}^{-2}$. The latter is consistent with $\nu^2 \approx 10^{-4} \text{ s}^{-2}$ found in this study (Sect. 4.4). Our estimates of F_v have an overall error of 20 %, which is mainly given by the K_z (Law et al., 2003).

Depth profiles of O_2/Ar are not available for our cruise. O_2/Ar ratios should be used for the calculation of F_v and F_e associated with biological O_2 fluxes. However, the error made by using O_2 concentrations instead of O_2/Ar is likely to be small, given that the vertical gradients in Ar saturation are probably small (Hamme and Severinghaus, 2007).

3.6 Mixed-layer oxygen mass balance

In this work we evaluate the influence of vertical fluxes on marine productivity estimates based on the O_2 budget

approach. The mixed-layer O₂ mass balance, as described by Emerson et al. (2008), and considering steady state, can be rewritten as

$$z_{\text{mix}} \frac{\partial c(\text{O}_2)}{\partial t} = G - R - F_g + F_v + F_e, \quad (7)$$

where $G - R = N$ and refers to the gross photosynthetic O₂ production minus the consumption oxygen by autotrophic and heterotrophic organisms present in the community. N is approximated from F_{bio} . In this O₂ balance budget, F_{bio} is used to account for physical effects instead of F_g . When the mass balance is expressed in terms of O₂/Ar, the first-order time derivative term on the left-hand side of Eq. (7) is not present (Kaiser et al., 2005). We also do not consider the air–sea flux of O₂ by bubbles as determining productivity from O₂/Ar ratios removes the need to quantify by this effect (Hamme and Emerson, 2006). Thus, Eq. (7) yields to $N = G - R + F_v + F_e$.

3.7 Estimates of gross photosynthetic O₂ production (G)

The method used here for estimates of G has been thoroughly presented and discussed recently by Juranek and Quay (2013). Fundamentally, G was constrained from the relative ¹⁷O/¹⁶O and ¹⁸O/¹⁶O isotope ratio differences between dissolved O₂ and air O₂ (¹⁷δ and ¹⁸δ), measured on the same discrete samples as used for the O₂/Ar calibration (Luz and Barkan, 2000).

The calculation follows the dual-delta method of Kaiser (2011), which assumes isotopic steady state and neglects horizontal and vertical mixing:

$$G = k_w c_{\text{eq}} \frac{(1 + {}^{17}\epsilon_E) \frac{{}^{17}\delta - {}^{17}\delta_{\text{eq}}}{1 + {}^{17}\delta} - \gamma_R (1 + {}^{18}\epsilon_E) \frac{{}^{18}\delta - {}^{18}\delta_{\text{eq}}}{1 + {}^{18}\delta} + \Delta(\text{O}_2) ({}^{17}\epsilon_E - \gamma_R {}^{18}\epsilon_E)}{\frac{{}^{17}\delta_P - {}^{17}\delta}{1 + {}^{17}\delta} - \gamma_R \frac{{}^{18}\delta_P - {}^{18}\delta}{1 + {}^{18}\delta}}, \quad (8)$$

where ϵ_E is the kinetic isotope fractionation during O₂ evasion, δ_{eq} is the relative isotope ratio difference between O₂ in equilibrium with the atmosphere and air O₂, δ_P is the relative isotope ratio difference between photosynthetic O₂ and air O₂, and $\gamma_R = {}^{17}\epsilon_R / {}^{18}\epsilon_R = 0.5179$ is the ratio of the ¹⁷O/¹⁶O to the ¹⁸O/¹⁶O respiratory fractionation (Luz and Barkan, 2005). For ¹⁸ε_E we use -2.8‰ (Knox et al., 1992) and assume ${}^{17}\epsilon_E = (1 + {}^{18}\epsilon_E)^{0.516} - 1 = -1.446\text{‰}$. Temperature dependent δ_{eq} values are calculated as ${}^{18}\delta_{\text{eq}} = e^{-0.00072951 + 0.42696T/K} - 1$ (Benson et al., 1979) and ${}^{17}\delta_{\text{eq}} = (1 + {}^{18}\delta_{\text{eq}})^{0.518} e^{(0.6\theta/^\circ\text{C} + 1.8)\text{ppm}} - 1$ (Luz and Barkan, 2009). The isotopic composition of photosynthetic O₂ is based on that of Vienna Standard Mean Ocean Water (VSMOW) (Barkan and Luz, 2011; Kaiser and Abe, 2012), the relative ¹⁷O/¹⁶O difference between seawater and VSMOW of -5ppm (Luz and Barkan, 2010) and measurements of the mean isotopic fractionation during photosynthesis by marine species of ${}^{17}\epsilon_P = 1.773\text{‰}$ and ${}^{18}\epsilon_P = 3.389\text{‰}$ (Eisenstadt et al., 2010).

A current disagreement in the literature regarding the isotope ratio difference between seawater and air O₂ shows values between ${}^{17}\delta_w = -11.888\text{‰}$ / ${}^{18}\delta_w = -23.324\text{‰}$ (Barkan and Luz, 2011) and ${}^{17}\delta_w = -12.107\text{‰}$ / ${}^{18}\delta_w = -23.647\text{‰}$ (Kaiser and Abe, 2012). Thus, we calculated two G values (G_1 and G_2) based on the two different sets of oxygen isotopic signatures resulting from photosynthetic activity (¹⁷δ_P and ¹⁸δ_P values) taken from Table 3 rows 6 m (¹⁷δ_P = -9.761‰ /¹⁸δ_P = -19.301‰) and 7 m (¹⁷δ_P = -9.980‰ /¹⁸δ_P = -19.625‰) in Kaiser and Abe (2012).

The ¹⁷O isotope excess (¹⁷Δ) of dissolved oxygen is also calculated according to the simplified form: ${}^{17}\Delta \equiv {}^{17}\delta - 0.5179 {}^{18}\delta$ (Eq. 4 in Kaiser, 2011). Although we no longer use ¹⁷Δ to calculate G (Kaiser, 2011), we report our results for presentational purposes.

The standard error in our ¹⁷Δ values is 3 ppm, with a population standard deviation of 9 ppm for the 11 aliquots of air-saturated water analyzed in the laboratory. The uncertainty in G estimated from the dual-delta method is partly due to the gas transfer coefficient, which is about 15% for typical oceanic mixed-layer conditions, and partly due to uncertainty in the isotope measurements.

Due to the lack of oxygen triple isotope measurements in waters below the mixed layer, corrections by F_v and F_e are not applied here to the G estimates. Furthermore, since respiration in waters below the mixed layer has little effect on the calculation of gross oxygen production using oxygen triple isotopes, we expect G to be less affected by entrainment than N .

4 Results

We present the results separately for WSIZ and POOZ. The WSIZ comprised two areas: (1) the coast of Wilkins Ice Shelf (WIS, CTD stations 1 to 36) south of the entrance to Marguerite Bay, and (2) Marguerite Bay 1 (MB1, CTD stations 178 to 198) close to the coast of Alexander Island. The POOZ comprised three areas: (1) Belgica Trough (BT, CTD stations 90 to 135), (2) Marguerite Bay 2 (MB2, CTD stations 199 to 213) in the northern part of the entrance to Marguerite Bay and towards the coast of Adelaide Island, and (3) west of Adelaide Island (WAI, CTD stations 214 to 252) in the northernmost part of the sampling area. The Marguerite Bay region was divided into two areas due to the contrasting distributions of the measured variables (Fig. 1).

Locations of the main water masses over depth in the area of study were identified with a T–S diagram (Fig. 2). Most of the water column contained AASW, followed by the more oxygenated MW. We also evaluated the relationship between the $c(\text{O}_2)$ and θ (in the entire water column, Fig. 4a; and only in the mixed layer Fig. 4c) and S (Fig. 4b and d).

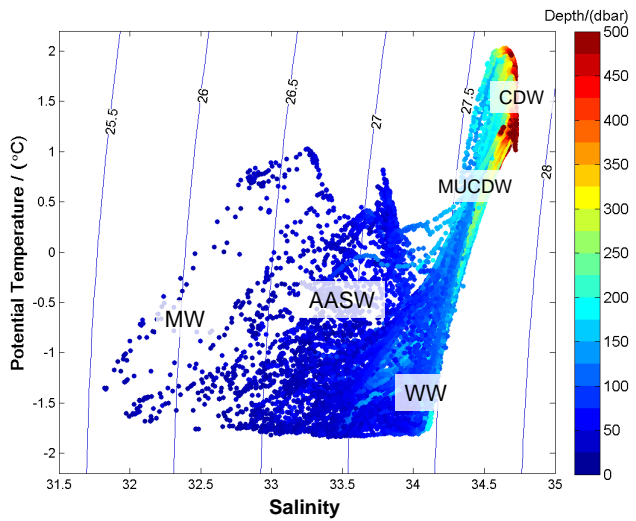


Fig. 2. T–S diagram derived from CTD profiles for identification of main water masses in the Bellingshausen Sea. Colors correspond to depth. MW, melt water; AASW, Antarctic surface water; WW, winter water; MUCDW, modified upper circumpolar deep water; and CDW, circumpolar deep water. Contours of potential density in sigma units ($\text{kg m}^{-3} - 1000$) are shown.

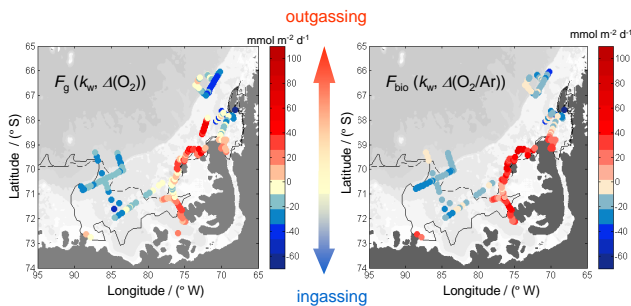


Fig. 3. Sea-to-air O_2 flux (F_g , left panel) and biological O_2 flux (F_{bio} , right panel), along the cruise track in the Bellingshausen Sea. The MIZ at the beginning (solid black contour) and at the end (dashed black contour) of the JR165 cruise are shown.

4.1 Variation of $\Delta(\text{O}_2/\text{Ar})$ in relation to the MIZ

The approximate location of the MIZ is shown in Fig. 1, and it was defined by a threshold sea ice concentration of 30%. Sea ice concentrations were obtained from 1 km resolution ENVISAT ASAR-E/ESA images (<http://www.seaice.dk>) at the beginning (3 March 2007) and end (4 April 2007) of the cruise. The change of the MIZ position between 95° and 87° W and 76° and 65° W was almost negligible. In contrast, a sea ice advance of about 215 km was observed in the central part of the area of study between 75° and 87° W, from the coast of Fletcher Peninsula, Allison Peninsula and Eltanin Bay towards the shelf break in Belgica Trough (Fig. 1). The rate of sea ice advance during the sampling period was about 5.6 km d^{-1} . This shows the formation of new ice with a fur-

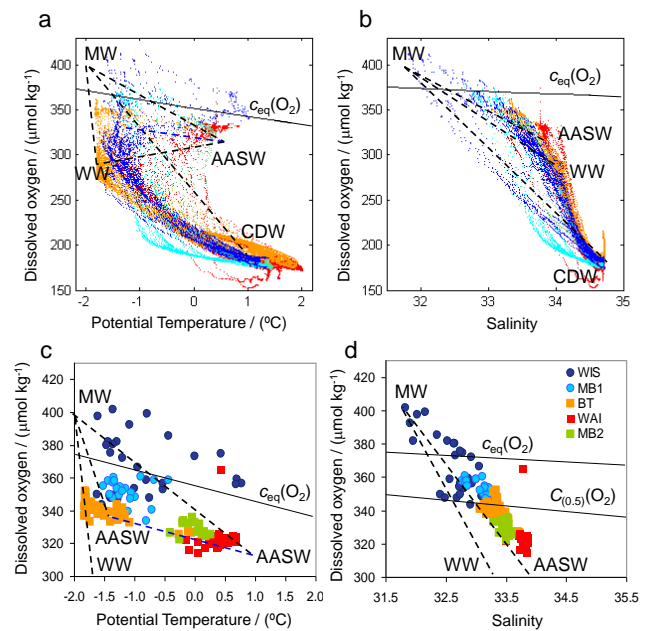


Fig. 4. Plots of dissolved oxygen against potential temperature and salinity. (a) and (b) include all measurements for identification of water masses; (c) and (d) only show mixed-layer data. Dashed lines correspond to the mixing lines given by the end points of properties for the different water masses. Solid lines show the O_2 concentrations at air saturation at (a, c) constant salinity of 33.5 and (b, d) constant temperature at seawater surface freezing point (-1.8°C). Note in panel (c) the blue dashed line represents the wide range of temperatures that characterize the AASW, extending from colder ($< -1.0^\circ\text{C}$) to warmer ($> 0.5^\circ\text{C}$) waters. (d) WIS and MB1 are supersaturated in O_2 , considering the range of temperature dominated in the mixed layer of these areas ($-1.8 < \theta < 0.5^\circ\text{C}$). $c(\text{O}_2)$ at these constant temperatures is depicted ($c_{\text{eq}}(\text{O}_2)$ at -1.8°C and $c_{(0.5)}(\text{O}_2)$ at 0.5°C).

ther advance of the MIZ towards the shelf break during the beginning of autumn.

During the cruise we made visual observations of the sea ice cover. Most of the stations located within the WSIZ presented open water conditions, with most of the first-year ice melted away towards the end of summer, and sparse ice floes can be seen. The only exception was station 22, located southwest of Charcot Island, where the ocean was covered predominantly by fast ice. The underway system onboard was shut down during this station and no dissolved gas data were acquired.

The spatial distribution of O_2 and O_2/Ar supersaturations in the WSIZ and POOZ was heterogeneous and clearly associated with the location of the MIZ. In the WSIZ, $\Delta(\text{O}_2)$ and $\Delta(\text{O}_2/\text{Ar})$ were $(2.4 \pm 3.0)\%$ and $(5.7 \pm 3.4)\%$, respectively (average $\pm 1\sigma$ and hereafter). In the POOZ, undersaturation prevailed, with $\Delta(\text{O}_2) = (-2.0 \pm 0.9)\%$ and $\Delta(\text{O}_2/\text{Ar}) = (-1.6 \pm 0.9)\%$. In the MB1 area, $\Delta(\text{O}_2/\text{Ar})$ was positive at $(5.3 \pm 2.9)\%$. In contrast, $\Delta(\text{O}_2/\text{Ar})$ in MB2 was

Table 1. Average (± 1 standard deviation) of the main measured and calculated variables in the mixed layer for cruise JR165 (summer 2007, Bellingshausen Sea). Results are categorized by area: WIS, Wilkins Ice Shelf; MB1, Marguerite Bay 1; BT, Belgica Trough; MB2, Marguerite Bay 2 and WAI, west of Adelaide Island (CTD stations in between the ones presented here are not included). Δz_{mix} is the change in mixed-layer depth over $\Delta t = 30$ days prior to sampling. Positive values indicate a deepening of the mixed layer. ν^2 is the Brunt-Väisälä frequency based on the density change in the top 50 m of the water column.

Area	CTD stations	$\theta/^\circ\text{C}$	S	$c(\text{O}_2)/(\mu\text{mol kg}^{-1})$	$\Delta(\text{O}_2)/\%$	$\Delta(\text{O}_2/\text{Ar})/\%$	$k_w/(\text{m d}^{-1})$	$\Delta z_{\text{mix}}/\text{m}$	z_{mix}/m	$(\Delta z_{\text{mix}}/\Delta t)/(\text{m d}^{-1})$	$10^4 \nu^2/(\text{s}^{-2})$
Winter sea ice zone (WSIZ)											
WIS	1–36	-0.9 ± 0.6	32.5 ± 0.4	367 ± 18	2.9 ± 3.6	6.2 ± 3.9	1.6 ± 0.4	-10 ± 4	14 ± 5	-0.3	1.5 ± 0.5
MB1	178–198	-1.1 ± 0.2	33.0 ± 0.2	352 ± 7	1.9 ± 2.5	5.3 ± 2.9	1.2 ± 0.3	4 ± 7	18 ± 7	0.1	1.2 ± 0.3
Permanent open ocean zone (POOZ)											
BT	90–135	-1.4 ± 0.4	33.3 ± 0.2	339 ± 5	-2.9 ± 0.6	-2.2 ± 1.0	2.0 ± 0.2	8 ± 7	28 ± 7	0.3	0.8 ± 0.3
MB2	199–213	-0.1 ± 0.1	33.5 ± 0.1	329 ± 4	-1.4 ± 1.1	-1.2 ± 0.9	2.8 ± 0.5	18 ± 10	34 ± 11	0.6	0.2 ± 0.1
WAI	214–252	0.4 ± 0.2	33.8 ± 0.1	323 ± 7	-1.8 ± 1.2	-1.5 ± 1.0	3.7 ± 0.4	21 ± 12	51 ± 14	0.7	0.04 ± 0.2

negative at $(-1.2 \pm 0.9)\%$. During the sampling period, the MIZ at the entrance of Marguerite Bay remained close to Alexander Island and towards George VI ice shelf (Fig. 1). Its location coincides with the contrasting $\Delta(\text{O}_2/\text{Ar})$ distribution between MB1 and MB2.

F_{bio} reflects the observed heterogeneity in $\Delta(\text{O}_2/\text{Ar})$ (Fig. 3). High biological O_2 fluxes were observed in the WSIZ, on average $(27 \pm 14) \text{mmol m}^{-2} \text{d}^{-1}$. In contrast, O_2/Ar undersaturations caused negative F_{bio} in the POOZ, on average $(-16 \pm 9) \text{mmol m}^{-2} \text{d}^{-1}$ (Table 2).

In the following sections, the properties of the upper 200 m are presented for the WSIZ (Sect. 4.2) and for the POOZ (Sect. 4.3). The stability of the water column is discussed (Sect. 4.4) and estimates of F_v and F_e are shown in Sect. 4.5. Gross oxygen production estimates are shown in Sect. 4.6, along with corresponding f ratios based on oxygen ($f = N/G$). Average values for various properties are summarized in Tables 1 and 2.

4.2 Winter sea ice zone (WSIZ)

In the WSIZ, the WIS area was sampled at the beginning of the survey during late summer (3 to 8 March 2007), while the MB1 area was sampled 28 days later representing early autumn (31 March to 2 April 2007). Despite the different sampling periods, the characteristics of the water column remained similar. In the WSIZ, MW dominated the top 80 m, including the mixed layer. MW was characterized by colder (-1.8°C), fresher ($S < 31.8$) and more O_2 -supersaturated water ($\Delta(\text{O}_2)$ up to 12%) than the waters below (Fig. 4c and d). Underneath, the water column was dominated by the saltier (33.5 to 34) and colder portion (-1.8 to -1.0°C) of AASW.

The mixed-layer depth (z_{mix}) was generally shallow with a mean of $(17 \pm 6) \text{m}$. In the WIS, temperature inversions occurred in the upper 50 m. The average change of temperature within the inversions ranged from -1 to 1°C over a few tens of meters. It is possible that the inversions were the result

of the horizontal advection of sea ice MW mainly from the coast of Charcot Island. Less MW influence was observed for Latady Island and Beethoven Peninsula, in the western and southern parts of WIS, respectively, and for Alexander Island in the north. AASW dominated the top 180 m near the coasts of Latady Island, Beethoven Peninsula and Alexander Island.

No remnant WW was found in the upper 100 m; this was expected as WW is replaced by AASW and MW during the summer. AASW was lying above modified upper circumpolar deep water (MUCDW, Fig. 2), with the latter located below 180 m and characterized by being warmer (0.5 to 0.8°C), saltier ($S > 34$) and undersaturated in O_2 by as much as 40%.

In the MB1 area, MW in the mixed layer appeared to originate from sea ice melt close to Alexander Island. MW extended horizontally and towards the northeast up to 31 km (from stations 194 to 199), and vertically up to 100 m depth. In the MB2 area between stations 199 and 201, MW penetrated as deep as 150 m. AASW dominated the mixed layer for the rest of the section towards Adelaide Island.

The monthly mean wind direction showed predominant southerly winds over the WIS and MB areas during February, March and April 2007. The weighted gas exchange coefficient (k_w) (Reuer et al., 2007; Sweeney et al., 2007) was 2 times lower in the WSIZ at $(1.4 \pm 0.3) \text{m d}^{-1}$ than in the POOZ at $(2.8 \pm 0.3) \text{m d}^{-1}$.

Positive net sea-to-air O_2 fluxes of (14 ± 7) and $(6 \pm 10) \text{mmol m}^{-2} \text{d}^{-1}$ were observed for WIS and MB1, respectively. The corresponding F_{bio} values were $(38 \pm 22) \text{mmol m}^{-2} \text{d}^{-1}$ for WIS and $(21 \pm 11) \text{mmol m}^{-2} \text{d}^{-1}$ for MB1 (Table 2 and Fig. 3).

4.3 Permanent open ocean zone (POOZ)

The observed MIZ advance towards the shelf break by the end of our cruise affected mainly the BT area, which was not fully sampled for underway O_2 and O_2/Ar (see Fig. 3), while

Table 2. Mixed-layer net and gross oxygen production and related variables. Positive F_g , F_v , F_e and F_{bio} values mean a net loss of oxygen from the mixed layer. Net community production is calculated as $N = F_{bio} + F_v + F_e$.

Area	$F_g/$ (mmol m ⁻² d ⁻¹)	$F_{bio}/$ (mmol m ⁻² d ⁻¹)	$F_v/$ (mmol m ⁻² d ⁻¹)	$F_e/$ (mmol m ⁻² d ⁻¹)	$N/$ (mmol m ⁻² d ⁻¹)	$^{17}\Delta/$ ppm	$G_1/$ (mmol m ⁻² d ⁻¹) ^a	$G_2/$ (mmol m ⁻² d ⁻¹) ^b	$f_1 =$ N/G_1	$f_2 =$ N/G_2	$N(C)/$ (mmol m ⁻² d ⁻¹)	$G(^{14}C)/$ (mmol m ⁻² d ⁻¹)	$f = N(C)/$ $G(^{14}C)$
Sea ice zone (SIZ)													
WIS	14 ± 7	38 ± 22	1.5 ± 1.1	0	39 ± 22	56 ± 25	231 ± 99	161 ± 58	0.17	0.24	28	73	0.39
MB1	6 ± 10	21 ± 11	3.1 ± 3.4	5 ± 6	29 ± 13	58 ± 9	181 ± 41	130 ± 29	0.16	0.22	21	58	0.37
Permanent open ocean zone (POOZ)													
BT	-23 ± 4	-18 ± 7	1.0 ± 0.9	6 ± 5	-12 ± 9	28 ± 9	139 ± 56	103 ± 40	(< 0)	(< 0)	(-8)	45	(< 0)
MB2	-13 ± 10	-12 ± 11	1.1 ± 1.9	15 ± 22	4 ± 25	25 ± 7	157 ± 31	118 ± 23	0.02	0.03	3	51	0.05
WAI	-23 ± 15	-20 ± 12	1.6 ± 3.3	22 ± 15	4 ± 20	24 ± 10	157 ± 61	118 ± 45	0.02	0.03	3	51	0.05

^a Calculated using $^{17}\delta_P = -9.761\%$ and $^{18}\delta_P = -19.301\%$ (Barkan and Luz, 2011; taken from Table 3 row 6 m in Kaiser and Abe, 2012).

^b Calculated using $^{17}\delta_P = -9.980\%$ and $^{18}\delta_P = -19.625\%$ (Kaiser and Abe, 2012; taken from Table 3 row 7 m in Kaiser and Abe, 2012).

the WAI and MB2 areas remained open during the sampling period.

In agreement with Vernet et al. (2008), we found that the mixed-layer depth increased with distance from the coast in the WAP region. The mixed-layer depth in the POOZ was on average 20 m deeper than in the WSIZ. Deeper and more variable mixed layers were observed in the WAI area (51 ± 14 m), while shallower mixed layers were found in the MB2 (34 ± 11 m) and the BT (28 ± 7 m) areas. This could be due to the stronger influence of northerly winds in the WAI area. The wind stress was weaker towards the coast, in the more topographically protected areas and towards the central part of the Bellingshausen Sea in the BT area during March and April.

The areas away from the coast had less influence of MW from the ice shelves, coastline and glaciers. The vertical profiles of temperature, salinity and dissolved oxygen indicate that the mixed layer was dominated by AASW. The latter is characterized by a wide range of temperatures (from the coldest at $-1.4\text{ }^\circ\text{C}$ in the BT away from the MW influence, followed by the MB2 with $0\text{ }^\circ\text{C}$, and finally WAI with $0.4\text{ }^\circ\text{C}$) (Fig. 4c). A consistent range of potential density between 1026.6 to 1027.2 kg m^{-3} was observed as a result of well-mixed upper water in this zone. AASW extended down to 180 m depth, above MUCDW. In agreement with Garibotti et al. (2003), the remnant of the WW was present between 50 and 100 m below the mixed layer and the seasonal pycnocline, where O_2 undersaturation levels up to 30 % were observed. A transect across the WAI showed WW beneath the mixed layer defined by the surface distribution of O_2 (Fig. 5).

In the POOZ, total O_2 was undersaturated, as was the biologically produced O_2 . The average $\Delta(\text{O}_2)$ was $(-2.0 \pm 0.9)\%$, corresponding to an O_2 concentration between 310 to $350\text{ }\mu\text{mol kg}^{-1}$, and $(-1.6 \pm 0.9)\%$ for $\Delta(\text{O}_2/\text{Ar})$ (Table 1). The O_2 concentration in the AASW was mainly close to saturation; however, it was slightly undersaturated at the higher temperature and salinity limits ($1\text{ }^\circ\text{C}$ and 33.7 ; Serebrennikova and Fanning, 2004). The lowest mixed-layer $\Delta(\text{O}_2)$ was -4% in the WAI area. The negative $\Delta(\text{O}_2/\text{Ar})$ values indicated net heterotrophy and/or mixing with undersaturated waters.

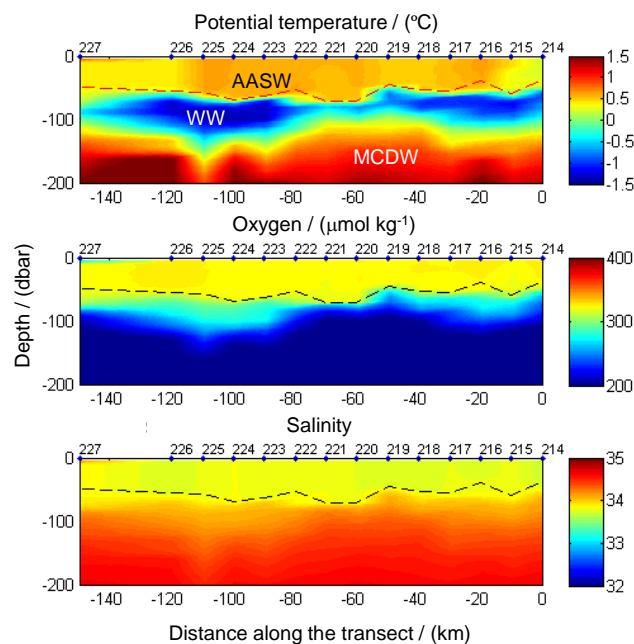


Fig. 5. Vertical sections showing the distribution of water masses for stations 214 to 227 in the west of the Adelaide Island area. The dashed horizontal line represents the bottom of the mixed layer as defined by the distribution of dissolved oxygen. AASW dominates the mixed layer, with WW beneath it and MCDW filling depths from 150 m.

The gas transfer coefficient was on average two times higher in the POOZ than in the WSIZ. The average F_g was $(-20 \pm 10)\text{ mmol m}^{-2}\text{ d}^{-1}$, and the average F_{bio} was $(-17 \pm 10)\text{ mmol m}^{-2}\text{ d}^{-1}$ (Table 2 and Fig. 3).

4.4 Stability of the water column

As a measure of water column stability, the square of the buoyancy frequency (Brunt-Väisälä frequency) was calculated as $\nu^2 \equiv -g/\rho\text{ d}\rho/\text{d}z$, where g is the acceleration due to gravity (9.81 m s^{-2}) and ρ the average seawater density in the top 50 m of the water column; these are multiplied by the change in density over the same depth range ($\text{d}\rho/\text{d}z$). We identified 50 m as the upper limit of the WW, consistent with

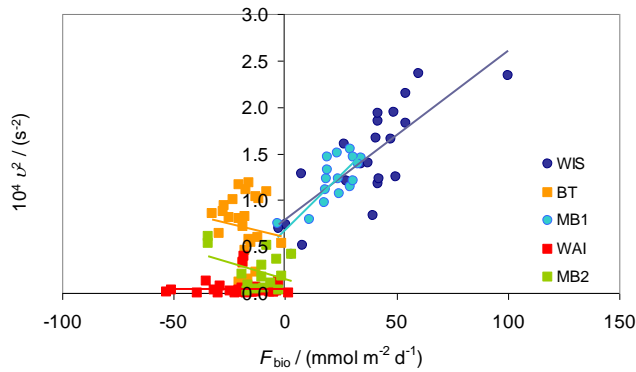


Fig. 6. Correlation between the square of the Brunt-Väisälä frequency ($10^4 \nu^2$) and the biological oxygen flux (F_{bio}): dark and light blue circles represent the stations located in the WIS and MB1 areas (WSIZ); squares in orange, green and red are the stations for the BT, MB2 and WAI areas, respectively, in the POOZ.

Garibotti et al. (2003). The upper 50 m of the water column in the continental shelf of the WAP experience the largest spatial variability due to local environmental processes (Hofmann and Klinck, 1998).

ν^2 in the POOZ was four times lower than in the WSIZ (Table 1). ν^2 averaged $1.5 \times 10^{-4} \text{ s}^{-2}$ and $1.2 \times 10^{-4} \text{ s}^{-2}$ in WIS and MB1, compared to $0.8 \times 10^{-4} \text{ s}^{-2}$, $0.2 \times 10^{-4} \text{ s}^{-2}$ and $0.04 \times 10^{-4} \text{ s}^{-2}$, in BT, MB2 and WAI, respectively. A positive correlation between ν^2 and F_{bio} was observed in the WSIZ areas ($R^2 = 0.61$ for WIS, and $R^2 = 0.63$ for MB1) (Fig. 6), consistent with previous observations of higher biological production associated with higher water column stability (i.e., Garibotti et al., 2003, 2005b; Smith et al., 1998; Vernet et al., 2008).

4.5 Calculation of N corrected by F_V and F_e

Often, F_{bio} is assumed to equal mixed-layer N (Hendricks et al., 2004; Reuer et al., 2007). However, as the values for F_V and F_e in Table 2 show, vertical mixing cannot be disregarded in the calculation of mixed-layer N in this region. Here we estimate N as the sum of F_{bio} , F_e and F_V , neglecting horizontal fluxes and assuming steady state. It is important to note that in all vertical profiles, the oxygen concentration below the mixed layer was consistently lower than in surface waters.

In the WSIZ areas, F_V was on average $(1.5 \pm 1.1) \text{ mmol m}^{-2} \text{ d}^{-1}$ for WIS and $(3.1 \pm 3.4) \text{ mmol m}^{-2} \text{ d}^{-1}$ for MB1. The positive F_V values mean that there is a net loss of O_2 from the mixed layer to the upper thermocline below. For the calculation of F_e , we estimated changes in mixed-layer depth from climatological data (de Boyer Montégut et al., 2004). According to these data, the WIS mixed layer may have been 10 m deeper 30 days prior to the occupation of this cruise section. Thus, F_e is zero because entrainment only occurs when the

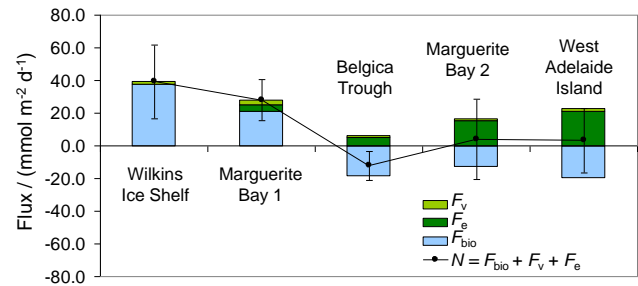


Fig. 7. Representation of O_2 fluxes (F_e , F_V and F_{bio} in $\text{mmol m}^{-2} \text{ d}^{-1}$) in the WSIZ and POOZ. Positive values indicate flux out of the mixed layer. The total N is depicted as a black line, with corresponding error bars representing the error after quantification of physical effects.

mixed layer deepens. With $F_V = 1.5 \text{ mmol m}^{-2} \text{ d}^{-1}$, vertical mixing is negligible in the WIS and $N = 39 \text{ mmol m}^{-2} \text{ d}^{-1}$ is almost equal to $F_{\text{bio}} = 38 \text{ mmol m}^{-2} \text{ d}^{-1}$. In contrast, the mixed layer in the MB1 area may have deepened by 5 m to 19 m. F_e and F_V in this area are (5 ± 6) and $(3.1 \pm 3.4) \text{ mmol m}^{-2} \text{ d}^{-1}$, respectively, suggesting O_2 loss from the mixed layer. N would therefore be about 1/3 higher than the observed F_{bio} value of $21 \text{ mmol m}^{-2} \text{ d}^{-1}$ and equal to approximately $29 \text{ mmol m}^{-2} \text{ d}^{-1}$. Thus, the WSIZ is characterized by net autotrophy during the sampling period.

F_V was similar in all areas of the POOZ: $(1.0 \pm 0.9) \text{ mmol m}^{-2} \text{ d}^{-1}$ for BT, $(1.1 \pm 1.9) \text{ mmol m}^{-2} \text{ d}^{-1}$ for MB2 and $(1.6 \pm 3.3) \text{ mmol m}^{-2} \text{ d}^{-1}$ for WAI (Table 2). According to the climatological data, z_{mix} was deeper at the time of sampling than 30 days before (Table 1) and the deepening occurred mainly within the extension of the AASW down into the water column in the BT and MB2 areas. However, in the WAI area where the deeper mixed layers during the sampling period were observed, the estimated deepening of the mixed layer by 4 m would reach the extension of the WW. N , corrected for F_V and F_e , was therefore $4 \text{ mmol m}^{-2} \text{ d}^{-1}$ in MB2 and WAI. Only the BT area, which is the furthest offshore, may have shown actual heterotrophy in the mixed layer with N of $(-12 \pm 9) \text{ mmol m}^{-2} \text{ d}^{-1}$.

The MB2 and WAI areas, rather than being net heterotrophic, may actually have been neutral or slightly autotrophic. In fact, the BT area may be the only net heterotrophic region after correcting for the physical effects. The advection of subsurface waters by entrainment appeared to have a higher effect on N in the MB2 and WAI than in BT by mixing and diluting mixed-layer waters with low-oxygenated subsurface waters (Table 2). The total fluxes for each area are depicted in Fig. 7.

4.6 G and ^{17}O excess in dissolved O_2

The highest $^{17}\Delta$ values in the area of study were found in the WIS and MB1 area, ranging between 31 to 81 ppm (Table 2).

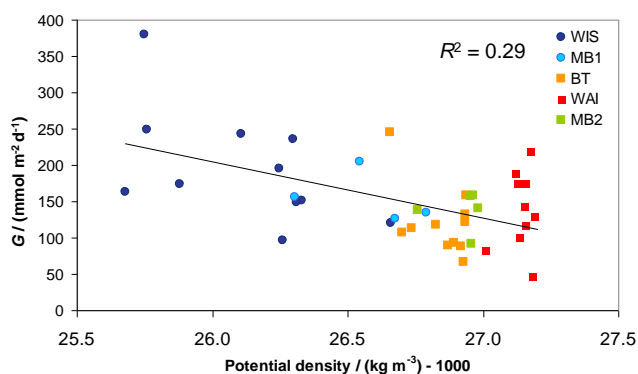


Fig. 8. Linear correlation ($R^2 = 0.29$) between potential density and mixed-layer average G .

On average, the $^{17}\Delta$ values were two times smaller in POOZ at (26 ± 9) ppm than in WSIZ at (57 ± 17) ppm.

G is calculated from oxygen triple isotope measurements. From the two G values (G_1 to G_2 given in Table 2) calculated using two different pairs of $^{17}\delta_P$ and $^{18}\delta_P$ (Kaiser and Abe, 2012), those based on Kaiser and Abe (2012) are about 40 % higher than the ones based on Barkan and Luz (2011) (Fig. 9). For the purposes of our discussion we use the mean of these two G values.

The mean of the G values is higher in WSIZ (176 ± 70 mmol m $^{-2}$ d $^{-1}$) than in POOZ (132 ± 49 mmol m $^{-2}$ d $^{-1}$). Sea ice melt water may have delivered enough nutrients to maintain higher productivity levels in the WSIZ areas, and at the same time contributed to increase the stratification of the water column. To evaluate this, mixed-layer potential density was compared to G (Fig. 8). A negative correlation ($R^2 = 0.29$) indicated that low potential densities (from 1025.7 to 1026.8 kg m $^{-3}$) generally corresponded with high mixed-layer G values. This is more evident in the WSIZ areas where the water column is more stable, with shallow z_{mix} and thus more light availability.

N and G were recalculated in carbon units. In WIS and MB1, $N(C)$ was equal to 28 and 21 mmol m $^{-2}$ d $^{-1}$, respectively; while $G(^{14}C)$ was equal to 73 and 58 mmol m $^{-2}$ d $^{-1}$, respectively. For the POOZ, $N(C)$ was equal to 3 mmol m $^{-2}$ d $^{-1}$ for MB2 and WAI, while $G(^{14}C)$ corresponded to 45 mmol m $^{-2}$ d $^{-1}$ in BT and 51 mg m $^{-2}$ d $^{-1}$ in MB2 and WAI (Table 2).

From the previous estimates, we calculated $f(O_2)$ ratios as $f = N/G$ (Table 2). This fraction is similar to the f ratio proposed by Eppley and Peterson (1979). The f ratio was defined by the authors based on nitrate assimilation rates relative to the total assimilation of nitrogen. The f ratio is an indicator of the ability of an ecosystem to retain or recycle organic matter by estimating the relative uptake of new versus total nitrogen (Eppley and Peterson, 1979). $f(O_2)$ ratio is expected to be about half the f ratio in terms of carbon since

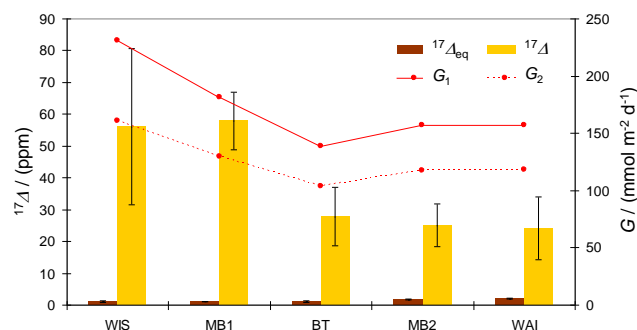


Fig. 9. Average ^{17}O excess ($^{17}\Delta$) (yellow bars, left axis) and G (red lines, right axis) in five areas in the Bellingshausen Sea. Brown bars represent the average ^{17}O excess at equilibrium with the atmosphere ($^{17}\Delta_{\text{eq}}$), calculated from in situ temperatures (Luz and Barkan, 2009). Two different sets of parameters have been used to calculate G_1 and G_2 (see main text for details).

$f(O_2) = 1.4 N(C)/2.7 G(^{14}C)$). For WIS the $f(O_2)$ ratio was on average 0.19 and for MB1 of 0.16. These values are notably higher than the ratio in the areas of the POOZ (0.02 for MB2 and 0.01 for WAI). In terms of carbon, the f ratio for the areas in the WSIZ corresponded to 0.37 and 0.30 for the WIS and the MB1, respectively, while for the POOZ it was 0.04 and 0.02 for MB2 and WAI.

5 Discussion

5.1 Influence of physical effects on N and G in the Bellingshausen Sea

In the WSIZ, the presence of shallow mixed layers in a sheltered geographical location less exposed to the wind stress is related to the stable water column and may support biological growth after the peak of the growing season. In the POOZ, the combination of stronger winds and the lesser influence of freshwater by lateral advection from ice shelves may explain a less stable water column. Perissinotto et al. (1990) suggested that local physical processes in the WAP control the accumulation and dissipation of phytoplankton communities, being a more important process for marine production than in situ growth.

The effect of physical processes on the N and G estimated using the O_2 budget approach in the Bellingshausen Sea cannot be neglected. In the POOZ, the $^{17}\Delta$ values were on average two times smaller than in the WSIZ. In the BT an apparent net heterotrophy is observed from the N values; however, the ^{17}O excess suggests the opposite with values well above the value in equilibrium with the atmospheric air (Fig. 9). This can be the result of the entrainment of waters below the mixed layer enriched in $^{17}\Delta$.

Similar observations were drawn from Hendricks et al. (2004): the authors suggested that the entrainment of oxygen-undersaturated waters does not have a large impact

on the upper $^{17}\Delta$ because the O_2 content in the entrained waters has already been low. The authors assumed that the $^{17}\Delta$ of the added O_2 is probably not far from the equilibrium value. Nevertheless, the results shown here suggest a possible incorporation of $^{17}\Delta$ from below the mixed layer as a result of the mixed-layer deepening. Despite the $\Delta(O_2)$ below the mixed layer during our sampling period being undersaturated due to respiration, the $^{17}\Delta$ in dissolved oxygen is not affected by this process (Luz and Barkan, 2000, 2009).

High $^{17}\Delta$ in waters below the mixed layer can result from diapycnal mixing or autogenic photosynthesis with limited loss of signal. During austral summer, the euphotic zone in the Southern Ocean can be deeper than the mixed layer. Huang et al. (2012) observed that the depth of the euphotic zone during summer was up to 37 m deeper than the mixed layer. Thus, photosynthetic O_2 can accumulate underneath the shallow summer mixed layer due to the attenuation of vertical mixing. Evidence of this process in nutrient content has been observed previously in the WAP (Serebrennikova and Fanning, 2004) and in the MIZ of the Australian sector of the Southern Ocean where nutrients remain stored below the summer mixed layer from the preceding winter mixed layer (Ishii et al., 2002).

As the season progresses and the mixed layer gets deeper towards autumn, the $^{17}\Delta$ excess of previously stored biological O_2 entrains into upper waters. Luz and Barkan (2009) observed $^{17}\Delta$ values above equilibrium with respect to air in samples from the Bermuda-Atlantic Time Series (BATS) station with the maximum production of $^{17}\Delta$ in the thermocline. The authors suggested that the high $^{17}\Delta$ must have been stored below the mixed layer before being delivered to waters above. Although in a different oceanic regime, similar processes might explain the high ^{17}O excess observed in the Bellingshausen Sea. However, due to the lack of $^{17}\Delta$ data below the mixed layer in our study, this hypothesis cannot be corroborated. To our knowledge, no depth profiles of $^{17}\Delta$ in the Southern Ocean have been published in the literature (Juraneck and Quay, 2013).

Entrainment of waters below the mixed layer and vertical diffusion can bias the mixed-layer productivity determination not only in the Bellingshausen Sea. Hamme and Emerson (2006), at the Hawaii Ocean Time-series station ALOHA, used the O_2 mass balance approach and concluded that vertical mixing below the mixed layer can lead to underestimating the N by up to 70 % at high mixing rates due to loss of O_2 from the mixed layer. Nicholson et al. (2012) evaluated the contribution of entrainment (considered by the authors as upwelling, diapycnal mixing and mixed-layer depth changes) in the subtropical gyres contributed to deliverance of thermocline water with high $^{17}\Delta$ content into the mixed layer. The authors concluded that neglecting the entrainment processes on productivity estimates can lead to overestimates by 60 to 80 % of annually averaged primary production in the subtropical gyre using the O_2 budget approach on a steady state.

Serebrennikova and Fanning (2004) observed during summer a high nutrient utilization away from the shore in Marguerite Bay. In this region we observed a decline of N which might have occurred towards early autumn and after the consumption of nutrients. Meredith et al. (2010) described the circulation pattern inside Marguerite Bay from observations of a time series of $\delta^{18}O(H_2O)$ measurements for seawater in order to trace the sea ice melt input to the ocean and the freshwater input from glacial and meteoric water in a site located in Marguerite Bay. The authors corroborated the heterogeneity of water properties in the bay with a higher influence of meteoric water during summer in northern MB (here MB2), compared with a contrasting oceanic influence due to the dominance of sea ice melt in the southern MB (here MB1). Our observations are in good agreement with Meredith et al. (2010) and Serebrennikova and Fanning.

5.2 Role of upwelling and lateral advection in the Bellingshausen Sea

Strength and direction of the wind play an important role in coastal upwelling, sea ice distributions and the resulting biological communities and distribution of O_2 . As a consequence of the predominant winds during our study, wind-driven coastal upwelling was most likely negligible during the sampling period. Smith et al. (2008) suggested that the dynamics in coastal waters of Marguerite Bay might have a strong influence on the marine productivity of this region by upward transport of CDW to the shelf from late summer to autumn. High levels of pigment biomass were encountered during the seasonal transition (Smith et al., 2008). This period is coincident with the sampling dates of the present study. Wallace et al. (2008) suggested that upwelling is intermittent in Marguerite Bay. From observations collected during the same time as cruise JR165 by a mooring located in the entrance of Marguerite Bay, the authors concluded that upwelling was only evident in March 2007, but not during the previous two months.

The strength and periodicity of upwelling at the continental shelf of the Bellingshausen Sea is unclear. Studies from moorings or tracers with high spatial resolution, such as oxygen, can help to elucidate O_2 budget (and N) of the Bellingshausen Sea.

Lateral advection is another important process that may affect the marine productivity in upper waters of the Bellingshausen Sea. Temperature inversions close to Charcot Island suggest lateral contribution of melt water from the coast into the mixed layer, which cannot be quantified based on our measurements.

5.3 Effect of ice on air–sea gas exchange

Sea ice might limit the air–sea gas exchange. Only sparse laboratory and field measurements have been performed so far in order to understand how sea ice affects the gas flux

between the ocean and the atmosphere (Fanning and Torres, 1991; Loose et al., 2009; Loose and Schlosser, 2011). Results of these experiments show an average moderate gas transfer reduction of about 25 % in the presence of up to 70 % ice cover and surface freshwater lenses with salinities between 10 and 33 (Fanning and Torres, 1991). It is unclear how the reduction of gas exchange scales with air–sea exchange (Loose and Schlosser, 2011) and there is currently no parameterization available for k in regions affected by sea ice. During our cruise the WSIZ was mainly characterized by open water with the presence of sparse ice floes – a typical condition towards the end of the melt season in this region. We encountered complete fast ice cover close to Charcot Island; however, the underway system onboard was shut down and no sampling for O_2/Ar and O_2 was done. The results presented here were taken at the end of the productive season, when sea ice was just starting to increase again. Since our gas exchange flux calculations were weighted over the 60 days prior to sampling, when sea ice cover would have been even less than we observed during the cruise, we do not consider a correction of air–sea exchange for sea ice to be appropriate.

5.4 Comparison with previous marine production estimates

To our knowledge the only published in vitro net community production measurements in the Bellingshausen Sea are those of Boyd et al. (1995). The authors derived depth-integrated N from dissolved oxygen changes in bottle incubations during November/December in 1993 at stations along $85^\circ W$ and between $70^\circ S$ and $67.5^\circ S$. Sampling season (late spring to beginning of summer compared to our sampling during the period of the end of summer to beginning of autumn) and geographical location (nearly 100 km north of our northernmost stations) differ from our study. Boyd et al. (1995) observed a retreat of the ice margin, whereas during our cruise the sea ice was advancing. We therefore limit the comparison with our results to the region that remained ice free during our sampling period (i.e., west of Adelaide Island, between 67° and $66^\circ S$ and 70° to $74^\circ W$). Boyd et al. (1995) reported a high chlorophyll feature at $67^\circ 30' S$ that was associated with a hydrographic front and not the retreating ice edge. This area with high rates of plankton metabolism was characterized by deep mixed-layer depths (up to 70 m) and a shallow euphotic layer (30 m) in station K, while a similar mixed-layer depth and euphotic zone were observed in station J (> 50 m). From the data in their Table 3, we derived mixed-layer N values of (181 ± 36) $mmol m^{-2} d^{-1}$ and (46 ± 22) $mmol m^{-2} d^{-1}$ (station K). Our N values of (4 ± 20) $mmol m^{-2} d^{-1}$ in the WAI area are considerably lower than the values from Boyd et al., and this is possibly due to the latter being obtained towards the peak of the growing season in contrast to our case. Despite the difference of our values, the biological oxygen flux in the WAI region of (-20 ± 12) $mmol m^{-2} d^{-1}$ on its own would not

have shown autotrophy without the correction we made due to entrainment.

A comparison of net community production estimates based on other methods, such as ^{14}C incubations, must be interpreted with caution (Juraneck and Quay, 2013; Robinson et al., 2009). Our measurements represent net community O_2 production, integrated over the mixed layer and the O_2 gas exchange time. In contrast, productivity derived from incubations approximates primary productivity integrated to the depth of the euphotic zone. Furthermore, net productivity estimated from satellite data represents only the top few centimeters of the water column and is integrated by numerical algorithms to the euphotic zone.

Vernet et al. (2008) estimated an integrated euphotic zone primary production for January of $745 mg m^{-2} d^{-1}$ ($62 mmol m^{-2} d^{-1}$) by averaging 12 yr of ^{14}C bottle incubations in the sea ice zone west of the Antarctic Peninsula. The data showed a maximum of $1788 mg m^{-2} d^{-1}$ ($149 mmol m^{-2} d^{-1}$) in 2006 and a minimum of $248 mg m^{-2} d^{-1}$ ($21 mmol m^{-2} d^{-1}$) in 1999. An onshore-offshore gradient of the estimated rates of net primary production was observed, particularly in the Marguerite Bay region, with the highest values at the mouth of the bay. The N values presented here for the WSIZ (mean of $24 mmol m^{-2} d^{-1}$) are closer to the minimum value; this is probably due to our measurements being performed in March to April, well after the peak of the growing season (January).

For the shelf areas of the Bellingshausen and Amundsen seas, Arrigo et al. (2008) estimated the highest mean daily primary production over a 9 yr period (1997 to 2006) as $316 mg m^{-2} d^{-1}$ ($158 mmol m^{-2} d^{-1}$). Their results are based on remotely sensed ocean color, sea surface temperature and sea ice concentration data. Their estimates are the highest for this area compared to the pelagic and MIZ zones and the results presented here are in close agreement.

High primary production (PP) in inshore regions of the WAP, compared to the ones beyond the shelf break have also been observed by others (i.e., Smith et al., 1998; Garibotti et al., 2003; Serebrennikova and Fanning, 2004; Mengesha et al., 2008). Agustí and Duarte (2005) confirmed that about $2 mmol m^{-3} d^{-1}$ is a threshold for gross primary production (GPP) to delineate the presence of net heterotrophic communities (i.e., where $R > GPP$) in the SO from O_2 measurements in a mesocosm experiment. For an average mixed-layer depth of 50 m, this value is equivalent to $100 mmol m^{-2} d^{-1}$, which is in close agreement to our G estimates in the POOZ ($110 mmol m^{-2} d^{-1}$) (Agustí and Duarte, 2005). Due to differences in the methods to estimate marine productivity so far applied in the WAP, the comparison to previous values of N and G in the Bellingshausen Sea is limited to results from the same approach used here. Hendricks et al. (2004) published results of N and G for samples collected in the Bellingshausen Sea during March in 2000. The authors show a decrease in the G values towards the south

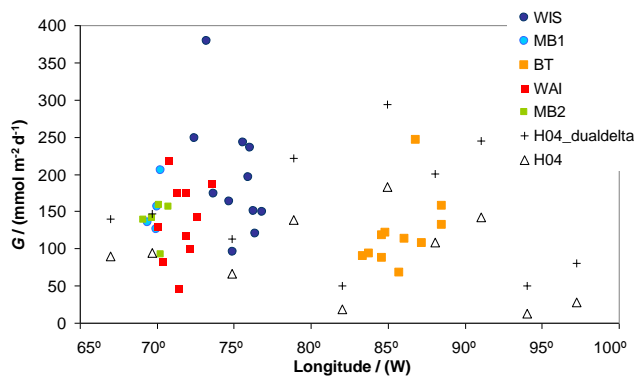


Fig. 10. Longitudinal distribution of G (average of G_1 and G_2). Comparison to results obtained by Hendricks et al. (2004) (H04) during March 2000 using $^{17}\Delta$ and recalculated values (H04_dualdelta) using $^{17}\delta$ and $^{18}\delta$.

(70° S) and west (98° W). The average G values shown by Hendricks et al. are about $25 \text{ mmol m}^{-2} \text{ d}^{-1}$, 5 times smaller than the values presented here. This difference is due to the $^{17}\Delta_{\text{eq}}$ value used for G calculation. The authors considered the standard value of +16 ppm (following Luz and Barkan, 2000), while here we estimated the $^{17}\Delta_{\text{eq}}$ independently for each sample, depending on their corresponding sea surface temperature.

For better comparison to this work, we have recalculated Hendricks' values. G was obtained, as in this work, from the dual-delta method following Eq. (8), along with the $^{18}\delta_{\text{eq}}$ parameterization by Benson et al. (1979) and $^{17}\Delta_{\text{eq}}$ from Luz and Barkan (2009). In their supplementary material presented by Reuer et al. (2007), the $^{17}\delta$ values were not reported, but were calculated from the given $^{17}\Delta$ and $^{18}\delta$ values. The concentration of oxygen was also not provided in the supplementary material; therefore, we calculated them from the $\Delta(\text{O}_2/\text{Ar})$ and $c_{\text{sat}}(\text{O}_2)$ provided. For this we assumed that $c(\text{Ar})$ equals $c_{\text{eq}}(\text{Ar})$; thus,

$$c(\text{O}_2) = c_{\text{eq}}(\text{O}_2) \times (\Delta(\text{O}_2/\text{Ar}) + 1). \quad (9)$$

The comparison of G between our results with the ones by Hendricks et al. (2004) following the traditional calculation based on ^{17}O excess and the recalculated G values from the dual-delta method, are depicted in Fig. 10. The recalculated values for gross oxygen production from Hendricks et al. are from only 11 discrete points distributed in the POOZ of the Bellingshausen Sea. Our results from discrete points distributed in the same zone (average of $156 \pm 65 \text{ mmol m}^{-2} \text{ d}^{-1}$), are in good agreement with the recalculated G values (average $154 \pm 84 \text{ mmol m}^{-2} \text{ d}^{-1}$). In all cases, the N values from Hendricks et al. (2004) were negative (average of $-25 \text{ mmol m}^{-2} \text{ d}^{-1}$), which is in close agreement with our F_{bio} values (before correction by physical effects) with an average of $-16.8 \text{ mmol m}^{-2} \text{ d}^{-1}$ for the POOZ.

From the observations made by Huang et al. (2012), it was not possible to recalculate G using the dual-delta method due to the lack of $^{17}\delta$, $^{18}\delta$ and $c(\text{O}_2)$ data in the supplementary material. Despite the different approach for calculation, and although the area of study by Huang et al. (2012) was located north of our area of study and mainly in the POOZ, the $^{17}\Delta$ values for the only overlapping section to our area of study and where data are available (i.e., in Huang et al. (2012) study transect line 200 consisting of 11 discrete data points off Marguerite Bay) are in close agreement with our results. The average $^{17}\Delta$ in Huang et al. (2012) is comparable (27 ± 22 ppm) to the mean $^{17}\Delta$ values obtained in this study for the WAI area (24 ± 10 ppm). In contrast to the results presented here, Huang et al. (2012) used $^{17}\Delta$ to estimate G ; thus, it is not possible to compare directly their results with our G estimates. In order to make an approximate comparison to G estimates, here we increased the G values from Huang et al. (2012) by 30 %, based on the observed difference from $^{17}\Delta$ G and dual-delta G values reported previously (Kaiser and Abe, 2012). Thus, the G values from Huang et al. (2012) following the dual-delta approach would correspond approximately to $(150 \pm 90) \text{ mmol m}^{-2} \text{ d}^{-1}$, while for the present study we obtained an average of $(142 \pm 54) \text{ mmol m}^{-2} \text{ d}^{-1}$ for the WAI area. In contrast, Huang reported that $\Delta(\text{O}_2/\text{Ar})$ remained low but positive (1.0 ± 0.8 %), whereas we observed negative $\Delta(\text{O}_2/\text{Ar})$ in the WAI area (-2.4 ± 0.9 %). This difference is probably due to the sampling time between both studies. While Huang's study occurred during the peak of the growing season, the present study occurred towards the beginning of autumn.

Several estimates for $f(\text{O}_2)$ ratios have been published and are compiled recently in Juranek and Quay (2013). Hendricks et al. in 2005 reported values for the equatorial Pacific with a mean of 0.06. Reuer et al. (2007) obtained an average value for $f(\text{O}_2)$ ratios equal to 0.13 in some regions of the Southern Ocean during summer. Luz and Barkan (2009) obtained values of 0.08 to 0.21 from samples collected at the BATS site in the Atlantic Ocean during May to October, 2000. Recently, Huang et al. (2012), reported $f(\text{O}_2)$ values for the WAP from -0.04 to 0.43, while Hamme et al. (2012) presented mean values between 0.08 and 0.12 in the Pacific sector of the Southern Ocean. Our results, with values from 0.02 at the POOZ and 0.2 at the WSIZ, are in agreement with the previous observations in the Southern Ocean and in other oceanic regions. This agreement is expected due to the large range of values reported so far in different regions of the global ocean (Hamme et al., 2012)

6 Conclusions and outlook

We presented high spatiotemporal resolution net community production from oxygen measurements in the Bellingshausen Sea. The distribution of N was found to be related

to the location of the marginal ice zone and water column stability. Diapycnal flux by diffusivity (F_v) is less important than (F_e), particularly in the POOZ. Net heterotrophy was restricted to offshore areas during the time frame that the mixed-layer N estimates represent in this work.

The results presented here are estimates of mixed-layer productivity as a snapshot for the seasonal transition from summer to autumn in 2007 integrated over the residence time of oxygen in the mixed layer. Despite the high uncertainty in the N estimates, the method used here was successful at identifying the high heterogeneity in marine productivity in the Bellingshausen Sea. Our results also highlight the importance of correcting for physical processes in regions where they have a large influence on the surface O_2 budget. Other processes, such as upwelling and lateral advection, should also be considered in the O_2 mass balance.

A predicted rise in temperatures and ice melting, as well as a delay of sea ice formation by strengthening of winds, can lead to an increase of the primary productivity along the coast in the Bellingshausen Sea. Lengthening the growing season towards autumn thanks to increased light availability may also extend the growing season.

Appendix A

In this Appendix we derive Eq. (6) used to estimate the influence of vertical mixing during entrainment of thermocline waters (F_e) when the mixed layer deepens.

Emerson et al. (2008) represented the entrainment flux due to a change of mixed-layer depth over the time ($\Delta z_{\text{mix}}/\Delta t$) as

$$F_e = (c_T - c_0) \frac{\Delta z_{\text{mix}}}{\Delta t}, \quad (\text{A1})$$

where c_T represents the concentration in the thermocline below the mixed layer and c the concentration in the mixed layer before the deepening event.

However, usually the concentration in the thermocline is not uniform. We therefore derive an equation that takes the concentration gradient below the bottom of the mixed layer into account. Since we are interested in O_2 , the relevant concentration gradient is the oxycline.

A simple mass balance describing the change of the mixed-layer O_2 inventory during mixed-layer deepening can be written as

$$z_{\text{mix}, 1} c_1 = z_{\text{mix}, 0} c_0 + \Delta z_{\text{mix}} c_T, \quad (\text{A2})$$

where Δz_{mix} is the change in mixed-layer depth ($\Delta z_{\text{mix}} = z_{\text{mix}, 1} - z_{\text{mix}, 0}$), and c_T in this case represents the average O_2 concentration of the entrained water from the oxycline.

Expressing the change in O_2 concentration as $\Delta c = c_1 - c_0$, Eq. (A2) can be written as

$$z_{\text{mix}, 1} \Delta c = \Delta z_{\text{mix}} (c_T - c_0). \quad (\text{A3})$$

Assuming a concentration gradient $\partial c(O_2)/\partial z|_{\text{oxy}}$ in the oxycline, the average concentration of the entrained water is

$$\begin{aligned} c_T &= \frac{1}{2} \left(c_0 + c_0 + \Delta z_{\text{mix}} \left. \frac{\partial c(O_2)}{\partial z} \right|_{\text{oxy}} \right) \\ &= c_0 + \frac{1}{2} \Delta z_{\text{mix}} \left. \frac{\partial c(O_2)}{\partial z} \right|_{\text{oxy}}. \end{aligned} \quad (\text{A4})$$

Thus,

$$z_{\text{mix}, 1} \Delta c = \frac{1}{2} (\Delta z_{\text{mix}})^2 \left. \frac{\partial c(O_2)}{\partial z} \right|_{\text{oxy}}, \quad (\text{A5})$$

and the entrainment flux is given by

$$F_e = z_{\text{mix}, 1} \frac{\Delta c}{\Delta t} = \frac{1}{2} \frac{(\Delta z_{\text{mix}})^2}{\Delta t} \left. \frac{\partial c(O_2)}{\partial z} \right|_{\text{oxy}}. \quad (\text{A6})$$

A decrease of O_2 with depth leads to a decrease of c in the mixed layer during mixing, corresponding to a negative sign for F_e . The approach relies on the assumption that the O_2 gradient in the oxycline at the time of sampling is the same as before the mixing event.

Supplementary material related to this article is available online at: <http://www.biogeosciences.net/10/2273/2013/bg-10-2273-2013-supplement.pdf>.

Acknowledgements. The British Antarctic Survey (BAS) and the Natural Environment Research Council supported this project through grant CGS8/29. K. C. M. thanks the National Council for Science and Technology (CONACyT), Mexico, for her PhD scholarship at the University of East Anglia. J. K. was also supported by a Royal Society Research Merit Award (WM052632). Special thanks to Adrian Jenkins (leader of ACES-FOCAS project) as well as to the participants and crew of cruise JR165. The authors would like to thank Michael Bender for allowing the analysis of the isotope samples at his lab in Princeton University. This work benefited from support provided to Michael Bender by the Office of Polar Programs of NSF and NASA.

The oxygen isotope data from this work can be found in the accompanying supplementary material. The hydrographic CTD data can be accessed by contacting co-author Deborah R. Shoosmith (drsho@bas.ac.uk).

Edited by: K. Suzuki

References

- Agustí, S. and Duarte, C. M.: Threshold of gross primary production for planktonic metabolic balance in the Southern Ocean: An experimental test, *Limnol. Oceanogr.*, 50, 1334–1339, doi:10.4319/lo.2005.50.4.1334, 2005.
- Arrigo, K. R., van Dijken, G. L., and Bushinsky, S.: Primary production in the Southern Ocean, 1997–2006, *J. Geophys. Res.*, 113, C08004, doi:10.1029/2007JC004551, 2008.
- Barkan, E. and Luz, B.: The relationships among the three stable isotopes of oxygen in air, seawater and marine photosynthesis, *Rapid Commun. Mass. Sp.*, 25, 2367–2369, doi:10.1002/rcm.5125, 2011.
- Bender, M., Orchardo, J., Dickson, M.-L., Barber, R., and Lindley, S.: In vitro O₂ fluxes compared with ¹⁴C production and other rate terms during the JGOFS Equatorial Pacific experiment, *Deep-Sea Res. I*, 46, 637–654, doi:10.1016/0967-0645(95)00068-2, 1999.
- Benson, B. B., Krause, D., and Peterson, M. A.: The solubility and isotopic fractionation of gases in dilute aqueous solution. I. Oxygen, *J. Solution Chem.*, 8, 9, 655–690, doi:10.1007/BF01033696, 1979.
- Boyd, P. W., Robinson, C., Savidge, G., and Williams, P. J. I.: Water column and sea-ice primary production during Austral spring in the Bellingshausen Sea, *Deep-Sea Res. II*, 42, 1177–1200, doi:10.1016/0967-0645(95)00070-7, 1995.
- Boyd, P. W., Watson, A. J., Law, C. S., Abraham, E. R., Trull, T. W., Murdoch, R., Bakker, D. C. E., Bowie, A. R., Buesseler, K. O., Chang, H., Charette, M., Croot, P., Downing, K., Frew, R., Gall, M., Hadfield, M., Hall, J., Harvey, M., Jameson, G., LaRoche, J., Liddicoat, M. I., Ling, R., Maldonado, M. T., McKay, R. M., Nodder, S., Pickmere, S., Pridmore, R., Rintoul, S. R., Safi, K., Sutton, P., Strzepek, R., Tanneberger, K., Turner, S., Waite, A., and Zeldis, J.: A mesoscale phytoplankton bloom in the polar Southern Ocean stimulated by iron fertilization, *Nature*, 407, 695–702, doi:10.1038/35037500, 2000.
- Cassar, N., Bender, M. L., Barnett, B., Fan, S., Moxim, W. J., Levy II, H., and Tilbrook, B.: The Southern Ocean biological response to aeolian iron deposition, *Science*, 317, 1067–1070, doi:10.1126/science.1144602, 2007.
- Cassar, N., DiFiore, P. J., Barnett, B. A., Bender, M. L., Bowie, A. R., Tilbrook, B., Petrou, K., Westwood, K. J., Wright, S. W., and Lefevre, D.: The influence of iron and light on net community production in the Subantarctic and Polar Frontal Zones, *Biogeosciences*, 8, 227–237, doi:10.5194/bg-8-227-2011, 2011.
- Castro-Morales, K. and Kaiser, J.: Using dissolved oxygen concentrations to determine mixed layer depths in the Bellingshausen Sea, *Ocean Sci.*, 8, 1–10, doi:10.5194/os-8-1-2012, 2012.
- Cook, A. J., Fox, A. G., Vaughan, D. G., and Ferrigno, J. G.: Retreating Glacier Fronts on the Antarctic Peninsula over the Past Half-Century, *Science*, 308, 541–544, doi:10.1126/science.1104235, 2005.
- Craig, H. and Hayward, T.: Oxygen supersaturation in the ocean: Biological versus physical contributions, *Science*, 235, 199–202, doi:10.1126/science.235.4785.199, 1987.
- de Boyer Montégut, C., Madec, G., Fisher, A. S., Lazar, A., and Iudicone, D.: Mixed layer depth over the global ocean: an examination of profile data and profile-based climatology, *J. Geophys. Res.*, 109, C12003, doi:10.1029/2004JC002378, 2004.
- Dickson, A. G.: Determination of dissolved oxygen in seawater by Winkler titration, in: WOCE Operations Manual, Volume 3: The Observational Programme, Section 3.1: WOCE Hydrographic Programme. Part 3.1.3: WHP Operations and Methods, edited by: World Ocean Circulation Experiment, Woods Hole, Massachusetts, USA, 1–13, 1996.
- Ducklow, H. W., Baker, K. S., Martinson, D. G., Quetin, L. B., Ross, R. M., Smith, R. C., Stammerjohn, S., Vernet, M., and Fraser, W.: Marine pelagic ecosystem: the West Antarctic Peninsula, *Philos. T. Roy. Soc.*, 362, 67–94, doi:10.1098/rstb.2006.1955, 2007.
- Eisenstadt, D., Barkan, E., Luz, B., and Kaplan, A.: Enrichment of oxygen heavy isotopes during photosynthesis in phytoplankton, *Photosynth. Res.*, 103, 97–103, doi:10.1007/s11120-009-9518-z, 2010.
- Emerson, S.: Seasonal oxygen cycles and biological new production in surface waters of the subarctic Pacific Ocean, *J. Geophys. Res.*, 92, 6535–6544, doi:10.1029/JC092iC06p06535, 1987.
- Emerson, S., Quay, P., Stump, C., Wilbur, D., and Schudlich, R.: Chemical tracers of productivity and respiration in the subtropical Pacific Ocean, *J. Geophys. Res.*, 100, 15873–15887, doi:10.1029/95JC01333, 1995.
- Emerson, S., Stump, C., and Nicholson, D.: Net biological oxygen production in the ocean: Remote in situ measurements of O₂ and N₂ in surface waters, *Global Biogeochem. Cy.*, 22, GB3023, doi:10.1016/j.dsr.2010.06.001, 2008.
- Eppley, R. W. and Peterson, B. J.: Particulate organic matter flux and planktonic new production in the deep ocean, *Nature*, 282, 677–680, doi:10.1038/282677a0, 1979.
- Fanning, K. A. and Torres, L. M.: ²²²Rn and ²²⁶Ra: indicators of sea-ice effects on air-sea gas exchange, *Polar Res.*, 10, 51–58, doi:10.1111/j.1751-8369.1991.tb00634.x, 1991.
- Garcia, H. E. and Gordon, L. I.: Oxygen solubility in seawater: better fitting equations, *Limnol. Oceanogr.*, 37, 1307–1312, doi:10.4319/lo.1992.37.6.1307, 1992.
- Garcia, H. E. and Gordon, L. I.: Erratum: Oxygen solubility in seawater: Better fitting equations, *Limnol. Oceanogr.*, 38, p. 656, 1993.
- Garibotti, I. A., Vernet, M., Ferrario, M. E., Smith, R. C., Ross, R. M., and Quetin, L. B.: Phytoplankton spatial distribution patterns along the western Antarctic Peninsula (Southern Ocean), *Mar. Ecol.-Prog. Ser.*, 261, 21–39, doi:10.3354/meps261021, 2003.
- Garibotti, I. A., Vernet, M., and Ferrario, M. E.: Annually recurrent phytoplanktonic assemblages during summer in the seasonal ice zone west of the Antarctic Peninsula (Southern Ocean), *Deep-Sea Res. I*, 52, 1823–1841, doi:10.1016/j.dsr.2005.05.003, 2005a.
- Garibotti, I. A., Vernet, M., Smith, R. C., and Ferrario, M. E.: Interannual variability in the distribution of the phytoplankton standing stock across the seasonal sea-ice zone west of the Antarctic Peninsula, *J. Plankton Res.*, 27, 825–843, doi:10.1093/plankt/fbi056, 2005b.
- Graham, A. G. C., Nitsche, F. O., and Larter, R. D.: An improved bathymetry compilation for the Bellingshausen Sea, Antarctica, to inform ice-sheet and ocean models, *The Cryosphere*, 5, 95–106, doi:10.5194/tc-5-95-2011, 2011.
- Guéguen, C. and Tortell, P. D.: High-resolution measurements of Southern Ocean CO₂ and O₂/Ar by membrane inlet mass spectrometry, *Mar. Chem.*, 108, 184–194, doi:10.1016/j.marchem.2007.11.007, 2008.

- Hamme, R. C. and Emerson, S. R.: The solubility of neon, nitrogen and argon in distilled water and seawater, *Deep-Sea Res. I*, 51, 1517–1528, doi:10.1016/j.dsr.2004.06.009, 2004.
- Hamme, R. C. and Emerson, S. R.: Constraining bubble dynamics and mixing with dissolved gases: Implications for productivity measurements by oxygen mass balance, *J. Mar. Res.*, 64, 73–95, doi:10.1357/002224006776412322, 2006.
- Hamme, R. C. and Severinghaus, J. P.: Trace gas disequilibria during deep-water formation, *Deep-Sea Res. I*, 54, 939–950, doi:10.1016/j.dsr.2007.03.008, 2007.
- Hamme, R. C., Cassar, N., Lance, V. P., Vaillancourt, R. D., Bender, M. L., Strutton, P. G., Moore, T. S., DeGrandpre, M. D., Sabine, C. L., Ho, D. T., and Hargreaves, B. R.: Dissolved O₂/Ar and other methods reveal rapid changes in productivity during a Lagrangian experiment in the Southern Ocean, *J. Geophys. Res.*, 117, C00F12, doi:10.1029/2011JC007046, 2012.
- Hendricks, M. B., Bender, M. L., and Barnett, B. A.: Net and gross O₂ production in the Southern Ocean from measurements of biological O₂ saturation and its triple isotope composition, *Deep-Sea Res. I*, 51, 1541–1561, doi:10.1016/j.dsr.2004.06.006, 2004.
- Hendricks, M. B., Bender, M. L., Barnett, B., Strutton, P. G., and Chavez, F. P.: Triple oxygen isotope composition of dissolved O₂ in the equatorial Pacific: A tracer of mixing, production, and respiration, *J. Geophys. Res.*, 110, C12021, doi:10.1029/2004JC002735, 2005.
- Hiraike, Y. and Ikeda, M.: Descending surface water at the Antarctic Marginal Ice Zone and its contribution to Intermediate Water: an ice-ocean model, *J. Oceanogr.*, 65, 587–603, doi:10.1007/s10872-009-0050-8, 2009.
- Hofmann, E. E. and Klinck, J. M.: Thermohaline variability of the waters overlying the west Antarctic Peninsula continental shelf, *Foundations for ecosystem research in the western Antarctic Peninsula region*, edited by: Ross, R., Hofmann, E. E., and Quentin, E., American Geophysical Union, Washington, DC, 61–80, 1998.
- Holland, P. R., Jenkins, A., and Holland, D. M.: Ice and ocean processes in the Bellingshausen Sea, Antarctica, *J. Geophys. Res.*, 115, C05020, doi:10.1029/2008JC005219, 2010.
- Holm-Hansen, O., Kahru, M., and Hewes, C. D.: Deep chlorophyll a maxima (DCMs) in pelagic Antarctic waters, II. Relation to bathymetric features and dissolved iron concentrations, *Mar. Ecol.-Prog. Ser.*, 297, 71–81, doi:10.3354/meps297071, 2005.
- Hopkinson, B., Greg Mitchell, B., Reynolds, R. A., Wang, H., Selph, K. E., Measures, C. I., Hewes, C. D., Holm-Hansen, O., and Barbeau, K. A.: Iron limitation across chlorophyll gradients in the southern Drake Passage: Phytoplankton responses to iron addition and photosynthetic indicators of iron stress, *Limnol. Oceanogr.*, 55, 2540–2554, doi:10.4319/lo.2007.52.6.2540, 2007.
- Howard, S. L., Hyatt, J., and Padman, L.: Mixing in the pycnocline over the western Antarctic Peninsula shelf during Southern Ocean GLOBEC, *Deep-Sea Res. II*, 51, 1965–1979, doi:10.1016/j.dsr2.2004.08.002, 2004.
- Huang, K., Ducklow, H. W., Vernet, M., Cassar, N., and Bender, M. L.: Export production and its regulating factors in the West Antarctica Peninsula region of the Southern Ocean, *Global Biogeochem. Cy.*, 26, GB2005, doi:10.1029/2010GB004028, 2012.
- Ishii, M., Inoue, H. Y., and Matsueda, H.: Net community production in the marginal ice zone and its importance for the variability of the oceanic pCO₂ in the southern Ocean south of Australia, *Deep-Sea Res. II*, 49, 1691–1706, doi:10.1016/S0967-0645(02)00007-3, 2002.
- Jacobs, S. S., Hellmer, H. H., and Jenkins, A.: Antarctic ice sheet melting in the Southeast Pacific, *Geophys. Res. Lett.*, 23, 957–960, doi:10.1029/96GL00723, 1996.
- Jenkins, A. and Jacobs, S. S.: Circulation and melting beneath George VI Ice Shelf, Antarctica, *J. Geophys. Res.*, 113, C04013, doi:10.1029/2007JC004449, 2008.
- Johnson, H. K.: Simple expressions for correcting wind speed data for elevation, *Coast. Eng.*, 36, 263–269, doi:10.1016/S0378-3839(99)00016-2, 1999.
- Juranek, L. W. and Quay, P. D.: Using triple oxygen isotopes of dissolved oxygen to evaluate global marine productivity, *Annual Review of Marine Science, Reviews in Advance*, 5, 10.11–10.22, doi:10.1146/annurev-marine-121211-172430, 2013.
- Kaiser, J.: Technical note: Consistent calculation of aquatic gross production from oxygen triple isotope measurements, *Biogeosciences*, 8, 1793–1811, doi:10.5194/bg-8-1793-2011, 2011.
- Kaiser, J. and Abe, O.: Reply to Nicholson’s comment on “Consistent calculation of aquatic gross production from oxygen triple isotope measurements” by Kaiser (2011), *Biogeosciences*, 9, 2921–2933, doi:10.5194/bg-9-2921-2012, 2012.
- Kaiser, J., Reuer, M. K., Barnett, B., and Bender, M. L.: Marine productivity estimates from continuous oxygen/argon ratio measurements by shipboard membrane inlet mass spectrometry, *Geophys. Res. Lett.*, 32, L19605, doi:10.1029/2005GL023459, 2005.
- Kana, T. M., Darkangelo, C., Hunt, M. D., Oldham, J. B., Bennett, G. E., and Cornwell, J. C.: Membrane inlet mass spectrometer for rapid high-precision determination of N₂, O₂, and Ar in environmental water samples, *Anal. Chem.*, 66, 23, 4166–4170, doi:10.1021/ac00095a009, 1994.
- Keeling, R. F. and Garcia, H. E.: The change in oceanic O₂ inventory associated with recent global warming, *Proc. Natl. Acad. Sci. USA*, 99, 7848–7853, doi:10.1073/pnas.122154899, 2002.
- Knox, M., Quay, P. D., and Wilbur, D.: Kinetic isotopic fractionation during air-water gas transfer of O₂, N₂, CH₄, and H₂, *J. Geophys. Res.*, 97, 20335–20343, doi:10.1029/92JC00949, 1992.
- Law, C. S., Abraham, E. R., Watson, A. J., and Liddicoat, M. I.: Vertical eddy diffusion and nutrient supply to the surface mixed layer of the Antarctic Circumpolar Current, *J. Geophys. Res.*, 108, 3272, doi:10.1029/2002JC001604, 2003.
- Laws, E. A.: Photosynthetic quotients, new production and net community production in the open ocean, *Deep-Sea Res.*, 38, 143–167, doi:10.1016/0198-0149(91)90059-O, 1991.
- Le Quééré, C., Rödenbeck, C., Buitenhuis, E. T., Conway, T. J., Langenfelds, R., Gomez, A., Labuschagne, C., Ramonet, M., Nakazawa, T., Metzl, N., Gillet, N., and Heimann, M.: Saturation of the Southern Ocean CO₂ sink due to recent climate change., *Science*, 316, 1735–1738, doi:10.1126/science.1136188, 2007.
- Loose, B. and Schlosser, P.: Sea ice and its effect on CO₂ flux between the atmosphere and the Southern Ocean interior, *J. Geophys. Res.*, 116, C11019, doi:10.1029/2010JC006509, 2011.
- Loose, B., McGillis, W. R., Schlosser, P., Perovich, D., and Takahashi, T.: Effects of freezing, growth, and ice cover on gas transport processes in laboratory seawater experiments, *Geophys. Res. Lett.*, 36, L05603, doi:10.1029/2008GL036318, 2009.

- Luz, B. and Barkan, E.: Assessment of oceanic productivity with the triple-isotope composition of dissolved oxygen, *Science*, 288, 2028–2031, doi:10.1126/science.288.5473.2028, 2000.
- Luz, B. and Barkan, E.: The isotopic ratios $^{17}\text{O}/^{16}\text{O}$ and $^{18}\text{O}/^{16}\text{O}$ in molecular oxygen and their significance in biogeochemistry, *Geochim. Cosmochim. Ac.*, 69, 1099–1110, doi:10.1016/j.gca.2004.09.001, 2005.
- Luz, B. and Barkan, E.: Net and gross oxygen production from O_2/Ar , $^{17}\text{O}/^{16}\text{O}$ and $^{18}\text{O}/^{16}\text{O}$ ratios, *Aquat. Microb. Ecol.*, 56, 133–145, doi:10.3354/ame01296, 2009.
- Luz, B. and Barkan, E.: Variations of $^{17}\text{O}/^{16}\text{O}$ and $^{18}\text{O}/^{16}\text{O}$ in meteoric waters, *Geochim. Cosmochim. Ac.*, 74, 6276–6286, doi:10.1016/j.gca.2010.08.016, 2010.
- Marra, J.: Approaches to the measurement of plankton production, in: *Phytoplankton Productivity: carbon assimilation in marine and freshwater ecosystems*, edited by: Williams, P. J. B., Thomas, D. N., and Reynolds, C. S., Blackwell Sci., Oxford, UK, 78–108, 2002.
- Martin, J. H., Gordon, R. M., and Fitzwater, S. E.: The case for iron, *Limnol. Oceanogr.*, 36, 1793–1802, doi:10.4319/lo.1991.36.8.1793, 1991.
- Matear, R. J., Hirst, A. C., and McNeil, B. I.: Changes in dissolved oxygen in the Southern Ocean with climate change, *Geochim. Geophys. Geosy.*, 1, 2000GC000086, doi:10.1029/2000GC000086, 2000.
- Meredith, M. P. and King, J. C.: Rapid climate change in the ocean west of the Antarctic Peninsula during the second half of the 20th century, *Geophys. Res. Lett.*, 32, L19604, doi:10.1029/2005GL024042, 2005.
- Meredith, M. P., Wallace, M. I., Stammerjohn, S., Renfrew, I. A., Clarke, A., Venables, H. J., Shoosmith, D. R., Souster, T., and Leng, M.: Changes in the freshwater composition of the upper ocean west of the Antarctic Peninsula during the first decade of the 21st century, *Prog. Oceanogr.*, 87, 127–143, doi:10.1016/j.pocean.2010.09.019, 2010.
- Montes-Hugo, M., Sweeney, C. G., Doney, S. C., Ducklow, H. W., Frouin, R., Martinson, D. G., Stammerjohn, S., and Schofield, O.: Seasonal forcing of summer dissolved inorganic carbon and chlorophyll *a* on the western shelf of the Antarctic Peninsula, *J. Geophys. Res.*, 115, C03024, doi:10.1029/2009JC005267, 2010.
- Mura, M. P., Satta, M. P., and Agustí, S.: Water-mass influences on summer Antarctic phytoplankton biomass and community structure, *Polar Biol.*, 15, 15–20, doi:10.1007/BF00236119, 1995.
- Nicholson, D. P., Stanley, H. R. R., Barkan, E., Karl, D. M., Luz, B., Quay, P. D., and Doney, S. C.: Evaluating triple oxygen isotope estimates of gross primary production at the Hawaii Ocean Time-series and Bermuda Atlantic Time-series Study sites, *J. Geophys. Res.*, 117, C05012, doi:10.1029/2010JC006856, 2012.
- Perissinotto, R., Duncombe Rae, C. M., Boden, B. P., and Allanson, B. R.: Vertical stability as a controlling factor of the marine phytoplankton production at the Prince Edward Archipelago (Southern Ocean), *Mar. Ecol.-Prog. Ser.*, 60, 205–209, doi:10.3354/meps060205, 1990.
- Pollard, R. T., Read, J. F., Allen, J. T., Griffiths, G., and Morrison, A. I.: On the physical structure of a front in the Bellingshausen Sea *Deep-Sea Res. II*, 42, 955–982, doi:10.1016/0967-0645(95)00064-W, 1995.
- Reuer, M. K., Barnett, B. A., Bender, M. L., Falkowski, P. G., and Hendricks, M. B.: New estimates of Southern Ocean biological production rates from O_2/Ar ratios and the triple isotope composition of O_2 , *Deep-Sea Res.*, 54, 951–974, doi:10.1016/j.dsr.2007.02.007, 2007.
- Robinson, C., Tilstone, G. H., Rees, A. P., Smyth, T. J., Fishwick, J. R., Tarran, G. A., Luz, B., Barkan, E., and David, E.: Comparison of in vitro and in situ plankton production determinations, *Aquat. Microb. Ecol.*, 54, 13–34, doi:10.3354/ame01250, 2009.
- Sea-Bird Electronics, I.: Application Note no. 64-3, Sea Bird Electronics 43 Dissolved oxygen (DO) sensor – hysteresis correction, Application Note no. 64-3, Sea-Bird Electronics, Inc., Sea-Bird Electronics, I., Bellevue, WA, 1–7, 2010.
- Serebrennikova, Y. M. and Fanning, K. A.: Nutrients in the Southern Ocean GLOBEC region: variations, water circulation, and cycling, *Deep-Sea Res. II*, 51, 1981–2002, doi:10.1016/j.dsr2.2004.07.023, 2004.
- Smith, W. O. and Comiso, J. C.: Influence of sea ice on primary production in the Southern Ocean: A satellite perspective, *J. Geophys. Res.*, 113, C05S93, 1–19, doi:10.1029/2007JC004251, 2008.
- Smith, D. A., Hofmann, E. E., Klinck, J. M., and Lascara, C. M.: Hydrography and circulation of the West Antarctic Peninsula Continental Shelf, *Deep-Sea Res. I*, 46, 925–949, doi:10.1016/S0967-0637(98)00103-4, 1999.
- Smith, R. C., Baker, K. S., and Vernet, M.: Seasonal and interannual variability of phytoplankton biomass west of the Antarctic Peninsula, *J. Marine Syst.*, 17, 229–243, doi:10.1016/S0924-7963(98)00040-2, 1998.
- Smith, W. O., Marra, J., Hiscock, M. R., and Barber, R.: The seasonal cycle of phytoplankton biomass and primary productivity in the Ross Sea, Antarctica, *Deep-Sea Res. II*, 47, 3119–3140, doi:10.1016/S0967-0645(00)00061-8, 2000.
- Smith, R. C., Martinson, D. G., Stammerjohn, S., Iannuzzi, R. A., and Ireson, K.: Bellingshausen and western Antarctic Peninsula region: Pigment biomass and sea-ice spatial/temporal distributions and interannual variability, *Deep-Sea Res. II*, 55, 1949–1963, doi:10.1016/j.dsr2.2008.04.027, 2008.
- Spitzer, W. S. and Jenkins, W. J.: Rates of vertical mixing, gas exchange and new production: Estimates from seasonal gas cycles in the upper ocean near Bermuda, *J. Mar. Res.*, 47, 169–196, doi:10.1357/002224089785076370, 1989.
- Sturm, M. and Masson, R. A.: 5. Snow and Sea Ice, in: *Sea Ice*, 2nd ed., edited by: Thomas, D. N. and Dieckmann, G. S., John Wiley & Sons Ltd., West Sussex, 621, 2010.
- Sweeney, C., Gloor, E., Jacobson, A. R., Key, R. M., McKinley, G., Sarmiento, J. L., and Wanninkhof, R.: Constraining global air-sea gas exchange for CO_2 with recent bomb ^{14}C measurements, *Global Biogeochem. Cy.*, 21, GB2015, 1–10, doi:10.1029/2006GB002784, 2007.
- Tortell, P. D.: Dissolved gas measurements in oceanic waters made by membrane inlet mass spectrometry, *Limnol. Oceanogr.-Meth.*, 3, 24–37, doi:10.4319/lom.2005.3.24, 2005.
- Tortell, P. D. and Long, M. C.: Spatial and temporal variability of biogenic gases during the Southern Ocean spring bloom, *Geophys. Res. Lett.*, 36, L01603, doi:10.1029/2008GL035819, 2009.
- Tortell, P. D., Guéguen, C., Long, M., Payne, C. D., Lee, P., and DiTullio, G. R.: Spatial variability and temporal dynamics of surface water pCO_2 , $\Delta\text{O}_2/\text{Ar}$ and dimethylsulfide in the Ross Sea, Antarctica, *Deep-Sea Res.*, 58, 241–259, doi:10.1016/j.dsr.2010.12.006, 2011.

- Tortell, P. D., Long, M., Payne, C. D., Alderkamp, A.-C., Dutrieux, P., and Arrigo, K. R.: Spatial distribution of $p\text{CO}_2$, $\Delta\text{O}_2/\text{Ar}$ and dimethylsulfide (DMS) in polynya waters and the sea ice zone of the Amundsen Sea, Antarctica, *Deep-Sea Res. II*, 71–76, 77–93, doi:10.1016/j.dsr2.2012.03.010, 2012.
- Turner, D. R. and Owens, N. J. P.: A biogeochemical study in the Bellingshausen Sea: overview of the STERNA 1992 expedition, *Deep-Sea Res. II*, 42, 907–932, doi:10.1016/0967-0645(95)00056-V, 1995.
- Vernet, M., Martinson, D., Iannuzzi, R., Stammerjohn, S., Kozłowski, W., Sines, K., Smith, R., and Garibotti, I.: Primary production within the sea-ice zone west of the Antarctic Peninsula: I-Sea ice, summer mixed layer, and irradiance, *Deep-Sea Res. II*, 55, 2068–2085, doi:10.1016/j.dsr2.2008.05.021, 2008.
- Wallace, M. I., Meredith, M. P., Brandon, M. A., Sherwin, T. J., Dale, A., and Clarke, A.: On the characteristics of internal tides and coastal upwelling behaviour in Marguerite Bay, west Antarctic Peninsula, *Deep-Sea Res. II*, 55, 2023–2040, doi:10.1016/j.dsr2.2008.04.033, 2008.